TRIBHUVAN UNIVERSITY

INSTITUTE OF ENGINEERING

PULCHOWK CAMPUS

THESIS NO.: M-397-MSREE-2023-2025

Modeling & Analyzing Heat Transfer Behavior of Sand Packed Bed Thermal Energy Storage System

by

Surendra Gurung

A THESIS
SUBMITTED TO THE DEPARTMENT OF MECHANICAL AND AEROSPACE ENGINEERING IN PARTIAL FULFILLMENT OF THE REQUIREMENTS FOR THE DEGREE OF MASTER OF SCIENCE IN RENEWABLE ENERGY ENGINEERING

DEPARTMENT OF MECHANICAL AND AEROSPACE ENGINEERING
LALITPUR, NEPAL

April, 2025

COPYRIGHT

TRIBHUWAN UNIVERSITY

INSTITUTE OF ENGINEERING

PULCHOWK CAMPUS

DEPARTMENT OF MECHANICAL AND AEROSPACE ENGINEERING

APPROVAL PAGE

The undersigned hereby certify that they have read, and recommended to the Institute of Engineering for acceptance, a thesis entitled **"Modeling & Analyzing Heat Transfer Behavior of Sand Packed Bed Thermal Energy Storage System"** submitted by Surendra Gurung in partial fulfillment of the requirements for the degree of Master of Science in Renewable Energy Engineering.

Supervisor, Assistant Professor Dr. Sanjeev Maharjan
Department of Mechanical and Aerospace Engineering
IOE, Pulchowk Campus, TU

External Examiner, Manisha Maharjan
Senior Divisional Engineer
Ministry of Education Science & Technology

Tribhuvan University
Institute of Engineering
Department of Mechanical and Aerospace Engineering
Pulchowk Campus

Committee Chairperson, Assistant Professor Dr. Sudip Bhattrai
Head, Department of Mechanical and Aerospace Engineering
IOE, Pulchowk Campus, TU

Date: April 10, 2025

ABSTRACT

This research investigates the heat transfer behavior of a sand-filled thermal energy storage (TES) system by designing and simulating a three-dimensional spatial model in COMSOL Multiphysics. Inspired by a physical test setup, the model uses sand as the TES medium, housed in an aluminum container with an outer plywood layer. For the heat transfer analysis, heat is supplied using two embedded resistance heaters in a sand-packed bed TES, which are raised to approximately 500°C and controlled within that temperature range using a heater thermocouple sensor and PID controller during the experiment. Temperature variations are recorded using thermocouples placed within the sand, capturing time-dependent temperature profiles at specific locations. The simulated temperature distribution using COMSOL Multiphysics is then assessed against experimental data.

Temperature predictions in the TES are obtained by solving the heat equation, with sand's effective thermal conductivity (ETC) determined using the effective medium method. Additionally, a secondary Excel-based numerical model is implemented to assess effective thermal conductivity, applying the Yagi-Kunii (YK) model, Kunii-Smith (KS), Zehner-Schlünder (ZS), Zehner-Bauer (ZBS), and Zehner-Damköhler correlations with radiation terms, allowing for comparison and validation of results. The modified Zehner -Bauer (ZBS) correlation, enhanced with radiative heat transfer components, yielded an ETC increasing from 0.16 to 0.34 W/(m .K) between 25-500°C, exhibiting a near-exponential growth trend influenced by thermal radiation at elevated temperatures. Implementing these conductivity values in the COMSOL model improves the agreement between simulated and experimental temperature distributions.

The investigation also examines the thermal conductivity enhancement of sand using scrap cast iron chips. Experiments were conducted to evaluate two integration techniques using aggregate and metallic chips mixed with sand. The results showed that incorporating 7.8% cast iron metallic chips (by volume) into the sand-aggregate mixture improved heat transfer, increasing the center temperature of the TES from 416°C to 448°C compared to pure sand. The TES with layered mixed sand aggregate with metallic chips was studied for 50 hours (0 to 49.5 hours) and it was noticed that during charging (0–5h), heater temperature reached 500°C in 1.3h (369°C/h), corresponding to initial sand heating at 96°C/h, showing thermal gradients with

charging rate at core (86°C/h) and in outer zone (T4: 46.8°C/h). In cooling (5–50h), temperatures dropped after a 1-hour delay, with the temperature briefly rising 12°C in between the heater and wall due to heat redistribution. The core (T2) cooled slowly (448°C→300°C in 11h), while the outer zone (T4) dissipated at 2.6°C/h, confirming effective heat retention and controlled release, making it suitable for long-term energy storage.

ACKNOWLEDGEMENT

Research is a collaborative endeavor, and this work would not have been possible without the support of many individuals. I extend my deepest gratitude to my supervisor, Assistant Prof. Dr. Sanjeev Maharjan, for his unwavering guidance, insightful feedback, and relentless encouragement throughout this research. His expertise and dedication were instrumental in refining the study's objectives and strengthening its outcomes. Our countless discussions and brainstorming sessions not only sharpened the focus of this work but also deepened my confidence as a researcher.

I would like to express my sincere gratitude to the Department of Mechanical and Aerospace Engineering for their unwavering support and coordination at every stage of this research. My heartfelt appreciation also extends to all the department professors for their invaluable guidance, insightful suggestions, and generous assistance throughout this project.

I extend my special appreciation to Maj Nitish Shrestha, Lt Sambat Basnet, and the entire School of EME, Nepali Army team for their invaluable assistance in the experimental setup, provision of critical data, and expert insights. Their contributions were indispensable to the success of this research.

Finally, I am profoundly grateful to my family for their endless encouragement and the supportive environment to complete my research work.

Surendra Gurung
PUL079MSREE018

TABLE OF CONTENTS

LIST OF TABLES

LIST OF FIGURES

LIST OF ABBREVIATIONS

CHAPTER ONE: INTRODUCTION

1.1 Background

As worldwide populations keep rising, so does the demand for food and energy. This rising energy demand is primarily met through burning fossil fuels, which is a significant concern due to their environmental impact. The International Energy Agency (IEA) reports that fossil fuels supply about 80 percent of the world's energy. However, they also contribute significantly to environmental issues, accounting for roughly 89% of global carbon dioxide (CO2) emissions and 75% of total greenhouse gas emissions, key factors fueling climate change and global temperature rise (Calvin et al., 2023). The urgent need to mitigate fossil fuel-derived CO2 and other greenhouse gas (GHG) emissions has necessitated accelerated development of clean energy resources, including photovoltaic, wind turbine, hydroelectric, bioenergy, and geothermal systems, to meet growing energy demand while significantly reducing emissions. These renewable energy sources are key to transitioning towards a low-carbon economy, helping to mitigate climate change and improve environmental sustainability (Calvin et al., 2023; IEA, 2023; IRENA, 2023). These renewable energy sources are considered crucial substitutes to fossil fuels because they produce energy without emitting greenhouse gases.

To keep Earth's warming under 2 degrees by reducing reliance on fossil fuels as pledged in the Paris Agreement, the International Renewable Energy Agency (IRENA) estimates that by 2030, renewable generation needs to supply 57% of worldwide power (IEA, 2023). As of 2022, the percentage composition of renewable generation in the global energy portfolio reached the highest ever recorded of 29%, reflecting the growing adoption of these sources. Projections indicate solar PV and wind energy will lead this growth, with renewable electricity generation projected to increase by roughly 18% and 17%, respectively, by 2023 (IEA, 2023; IRENA, 2023). Unlike conventional power, photovoltaic and wind energy systems pose intermittency issues. The sun is only available during the day and can be obscured by clouds, while the wind can vary in strength and may not blow at all times. The unpredictable supply variability of these renewable energies poses a challenge to couple them into the grid, requiring advanced energy storage systems (ESSs) solutions to keep the power supply stable and reliable

(Mitali et al., 2022). Among various ESSs, TES systems stand out as a cost-effective solution. These systems efficiently store thermal energy for later use, reducing the reliance on more expensive battery technologies and optimizing available resources (Sunku Prasad et al., 2019; Tetteh et al., 2021). TES systems generally have lower upfront costs than mechanical, electrical, electrochemical, or hydrogen storage methods, because of their less complex infrastructure and material needs. Additionally, they often incur fewer maintenance expenses over their operational lifespan. This makes TES systems a more cost-effective option for energy storage (Alva et al., 2017; Villasmil et al., 2019). The economic advantage of TES systems is their use of simple, easily obtainable materials like crushed rock, liquid salt compounds, fine sand, and other phase-change materials (PCMs). Unlike more complex storage technologies, which require rare or processed components, these materials are affordable and scalable, helping reduce overall system costs. This lower cost comes mainly from using simple, widely available materials like salts, sand, rocks, or phase-change materials. These materials are less expensive than those used in other storage technologies. As a result, TES systems can offer a more economical solution for energy storage (Lou et al., 2021). This scalability contributes to making TES systems an even more cost-effective option. Given the increasing need for flexible and responsive energy solutions in a grid dominated by renewables, the economic feasibility of TES makes it a critical solution for balancing variable renewable generation, accelerating the shift to decarbonized energy systems (Al-Ghussain et al., 2022).

1.2 Problem statement

The accelerating global transition to renewable energy has increased the need for dependable and eco-friendly storage solutions for power management to manage the variability of energy sources like solar and wind, making this need more pressing than ever (IEA, 2023). Although significant progress has been made, a major issue still stands: the unavailability of sunlight for solar power and the unpredictability of wind situations for wind power. As a result, having reliable energy storage solutions is crucial to storing surplus energy produced during high-generation intervals for utilization during production shortfalls. Traditional battery technologies are effective but constrained by their high costs, limited material availability, and environmental concerns, which have raised questions about their scalability and long-term viability.

TES systems help solve this through the accumulation of thermal energy, which doesn't fade quickly and can be used on demand. Among the various TES technologies, sand-packed bed TES, which utilizes the inherent heat capacity of sand for long-term energy storage, offers a promising solution. Sand is abundant, inexpensive, and possesses excellent thermal retention properties, making it a worthwhile option for large-scale energy storage (Polar Night Energy, n.d.-b). Despite its potential as a TES medium, sand's relatively low thermal conductivity presents a major limitation for system efficiency. Despite the potential benefits, there is a critical gap in research focused on optimizing TES materials. This research seeks to explore how to improve sand's thermal conductivity through the incorporation of metallic additives can enhance TES efficiency. By advancing these technologies, the study aims to contribute to more reliable and sustainable energy systems, helping the world cut carbon emissions and fight climate change.

1.3 Research Objectives

1.3.1 Main objective

To model and analyze the heat distribution behavior of a sand-filled thermal energy storage (TES) system.

1.3.2 Specific objectives

- To design a sand-filled TES system for studying heat transfer characteristics inside TES.
- To simulate a sand-filled TES system for analysis of the heat transfer behavior inside it.
- To perform an experimental study of a sand-filled TES prototype and enhance thermal conductivity using aggregate and scrap cast iron metallic chips.

1.4 Limitations & Assumptions

The model proposed in this work will be validated via side-by-side examination with experimental data from a single experiment, which could limit both the experimental and modelling perspectives in the following ways.

- Experimental limitations could include errors in the measurement apparatus as well as limitations of the experimental design.

- In model development, various material property values are sourced from the literature. This can be a limitation since material properties tested under different conditions may yield varying results. Thus, it is essential to carefully choose literature values for material properties.

The experimental limitations are reduced by careful design, thorough equipment testing, and conducting repeated trials to accomplish a reasonable level of confidence in the observed results. High-quality material property values and parametric studies are used to refine modeling accuracy.

CHAPTER TWO: LITERATURE REVIEW

This literature review will provide a foundation for developing a 3-dimensional numerical model using the finite element method (FEM) and conducting experimental work to obtain time-dependent temperature curves at critical points in the TES system. This review explores the key parameters affecting temperature in TES systems, specifically those utilizing sand beds for thermal conductivity enhancement. The study will review existing research on TES systems, focusing on sand bed thermal conductivity improvements.

2.1 Energy Storage Systems

Energy storage systems (ESS) act as a key component in maintaining modern power grids by storing surplus energy for a longer duration when production is high and releasing energy in the form of electricity when demand spikes or supply drops, thereby ensuring consistent grid operation. Through the mitigation of power variability, ESS enhances grid stability and decreases dependence on fossil fuel peaking plants, improving the dependability and efficiency of renewable energy integration (Mitali et al., 2022). These technological improvements allow better renewable energy utilization by storing excess production, regulating voltage and frequency instabilities in the power grid. As a result, a fully renewable energy grid is becoming increasingly attainable (Al-Ghussain et al., 2022). Lithium-ion batteries demonstrate unparalleled energy storage capacity, long-term durability, and fast recharge performance, make them the dominant technology powering the e-mobility revolution (Chen et al., 2020; Olivetti et al., 2017). Meanwhile, alternative ESS such as TES are emerging as cost-effective and resource-efficient options for stationary electric-grid storage applications. TES can substitute lithium-ion batteries, thereby reducing storage costs and making better use of limited materials and resources. This shift towards diverse ESS technologies is critical for delivering clean energy solutions that are environmentally sustainable and commercially competitive (Kebede et al., 2022).

2.2 TES and Classification

The TES system works by storing thermal heat when the energy generation system is on by charging and releasing it when needed during discharging. This process relies on

how thermal energy naturally spreads from warmer objects to cooler ones whenever there's a temperature difference between two objects. Heat can be transferred via three mechanisms: conductive contact between materials, convective fluid motion, or radiative electromagnetic waves (Dinçer & Rosen, 2010). TES is generally categorized into heat storage methods like sensible, latent, and thermochemical systems.

Sensible heat storage functions by heating a medium like water or sand, storing energy through temperature increase. The stored energy is influenced by the medium's storage mass, specific heat capacity, and the difference in temperature (Alva et al., 2018). While this is a simple, durable method that offers cost-effective advantages, its energy density may fall below alternative TES approaches. Energy is accumulated by elevating the temperature of solid or liquid media (e.g., water, concrete). The storage capacity scales with the medium's ΔT, mass, and Cp, making these properties critical for material selection (Dinçer & Rosen, 2010). The governing thermodynamic relationship is:

$$Q = m \times Cp \times \Delta T \qquad \text{Eq. 2.1}$$

Sensible TES systems commonly utilize materials that offer high thermal capacity and cost-effectiveness. As shown in Figure 2.1, sensible TES system efficiency is enhanced through adaptable configurations and optimized heat exchanger arrangements.

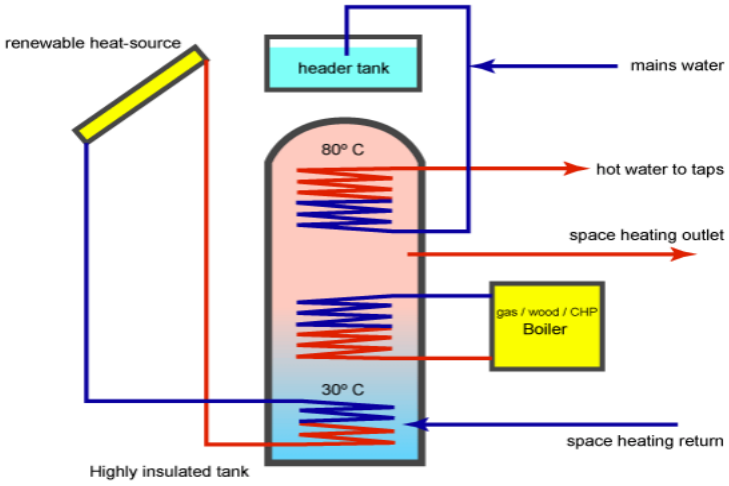

Figure 2.1: Heat energy stored in the water tank(Greenspec, 2024).

Latent heat TES, in contrast, offers more energy in less space by storing heat when materials melt or solidify. These materials are called phase change materials (PCMs),

which retain and discharge significant thermal energy as they change between solid and liquid states. Due to their poor thermal conductivity, PCM-based systems often experience extended charge/discharge durations (Lin et al., 2023).

Thermochemical energy storage (TCES) corresponds to the third TES category, which exploits reversible chemical processes (metal oxidation, ammonia cycles) for thermal storage. Despite their potential for exceptional storage capacity and cycle stability, these systems currently face technological challenges (Lin et al., 2023).

When talking about TES systems, we often focus on how they store energy through sensible, latent, or thermochemical heat. But there's more to it than just the storage method. TES systems can also be understood by looking at how they're charged, how heat is transferred, or what kind of reservoir they use. For example, in active TES systems, heat is added to the system through some form of work, such as circulating a heat transfer fluid (HTF) through the storage material. Conversely, passive systems operate differently, by exploiting convective heat transfer and thermal buffering. A prime example of passive TES is how brick walls in a building gradually soak up heat during sunny days and slowly release it at night, naturally balancing indoor temperatures (Alva et al., 2018).

As shown in Figure 2.2, the Classification of TES distinguishes between direct and indirect approaches. Direct systems employ a unified medium, like mineral oils, that functions simultaneously as a heat transfer fluid (HTF) and thermal storage medium, contained within specialized reservoirs. However, this method can be costly because it requires large quantities of potentially expensive heat transfer fluid. In contrast, indirect TES involves separate mediums for thermal exchange and storage. For example, a heat transfer fluid (HTF) like water is circulated to conduct thermal energy into a particulate storage medium (e.g., sand or gravel), which is then retained in an insulated reservoir (Alva et al., 2018).

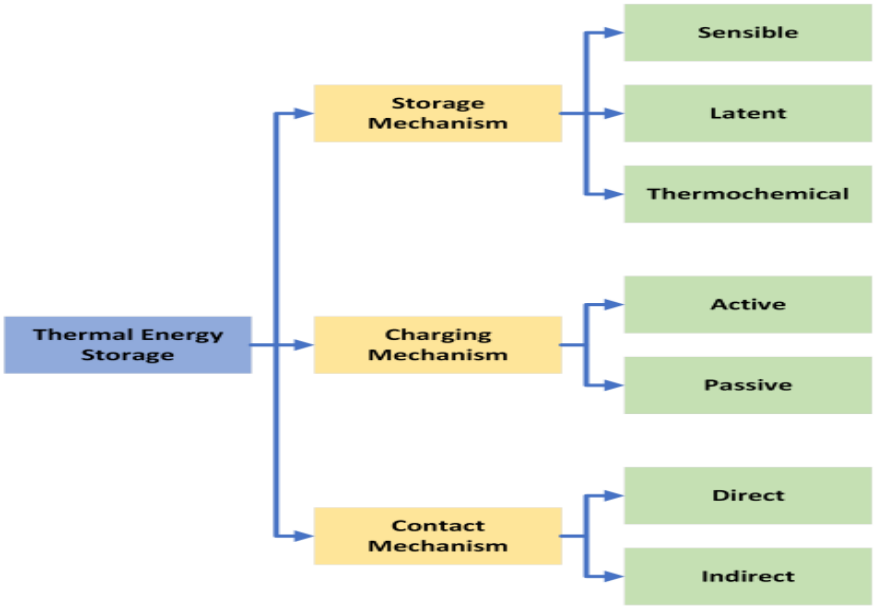

Figure 2.2: Classification of TES systems (Alva et al., 2018).

The TES system explored in this study consists of a densely packed sand bed that operates without the need for HTF (Tetteh et al., 2021). Rather than using a heat transfer fluid, the system undergoes direct Joule heating via electrical resistance elements embedded within the sand. This design eliminates the need for pumping and decreases the heat exchanger expenses commonly found in traditional TES systems. However, for optimal performance, the packed bed material must have sufficient thermal conductivity and be well-optimized for efficient heat storage and release.

2.3 Sand as a TES Medium

Examining the practical design of a TES system, Polar Night Energy specializes in developing TES system solutions for industrial applications. Their system utilizes sand as a storage medium, heating it to temperatures ranging from 600°C to 1000°C. The thermal battery reportedly provides 10 MW of power output and can store 1,000 MWh of energy (Polar Night Energy, n.d.-a).

Sand's most notable qualities include its abundance, low cost, and wide operating temperature range. The specific heat of sand shows a positive temperature dependence, with an average value of 980 J/(kg·K) across the tested samples within the 200°C to 1100°C range. The heat capacity exhibits a noticeable maximum at approximately 575°C, caused by the alpha-to-beta quartz transition (Diago et al., 2016). Exceeding

this temperature threshold could optimize the sand's storage potential by leveraging this thermal behavior.

2.4 Modelling Heat Transfer in Granular Mediums

Modeling heat flow in a granular material-filled thermal energy storage (TES) can be complex, but simplified methods can make the process more manageable. These models primarily focus on tracking temperature changes within the storage material over time, using the heat equation to predict how heat spreads and dissipates:

$$\rho C_p \frac{\delta T}{\delta t} - k\nabla^2 T = Q \qquad \text{Eq. 2.2}$$

heat equation incorporates: T (temperature, K), ρ (density, kg/m³), Q (heat source, W/m³), Cp (specific heat capacity, J/(kg·K)), k (thermal conductivity, W/(m·K)), and t (time, s) to describe the storage medium's thermal behavior. While 3D simulations provide deeper insights into thermal storage behavior, including geometric effects, they are computationally exhaustive and numerous parameter inputs, often requiring experimental support (Liang et al., 2022).

Two-phase thermal models separately analyze the solid particle and fluid phases while considering their interactive heat transfer processes. These simulations must incorporate multiple thermal transport phenomena that occur at the particle-fluid interface, as demonstrated in Figure 2.3. The key mechanisms involve: (1) radiative and conductive heat transfer between adjacent particles, (2) conductive pathways through individual particles and their contact points, and (3) convective heat transfer through the interstitial fluid regions.

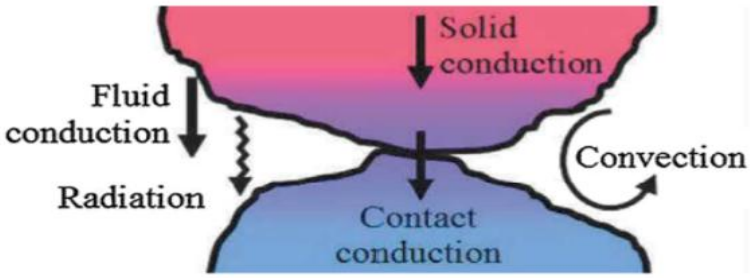

Figure 2.3: Interacting conduction, convection and radiation mechanisms in packed granular media (Díaz-Heras et al., 2020).

This study examines a sand-based TES that functions without an HTF, eliminating the need for fluid flow models. To enhance its utility as a design tool, the model is developed in 3D. Simulating the system as a two-phase medium, with separate calculations for sand grains and air, is too complex for practical computation, and simple one-dimensional models don't provide accurate results. Instead, researchers use the Effective Medium Technique, which treats the sand-air mixture as a single, uniform material. This approach simplifies the heat transfer process by combining various factors into a single parameter: effective thermal conductivity. Similarly, the overall properties of the material are averaged to make calculations more manageable.

Solving the heat equation for TES temperature profiles requires thermal conductivity data. The Effective Medium Technique replaces granular heat transfer mechanisms with a single effective thermal conductivity (ETC), for which researchers have developed multiple empirical correlations to predict the ETC of packed beds.

Yagi-Kunii (YK) Model

The unit cell derived by Yagi and Kunii evaluates thermal conductivity by integrating various heat transfer mechanisms, including solid-phase conduction, contact-point conduction between particles, surface-to-surface radiation, radiative transfer through voids, fluid-film conduction around solids, micro-scale convection in particle gaps, and macro-scale convective mixing (under flow conditions).

The model demonstrates that mechanisms 1–5 remain unaffected by fluid dynamics, while mechanism 6 contributes insignificantly compared to the other pathways. Moreover, mechanisms 1–5 operate independently of mechanisms 6 and 7. Consequently, under static (no-flow) conditions, the effective thermal conductivity (ETC) is governed exclusively by mechanisms 1–5 (Yagi & Kunii, 1957). As shown in Figure 2.4, the numerical labels appear in descending order as 2, 3, 1, 5, and 4, referencing the previously listed heat transfer pathways.

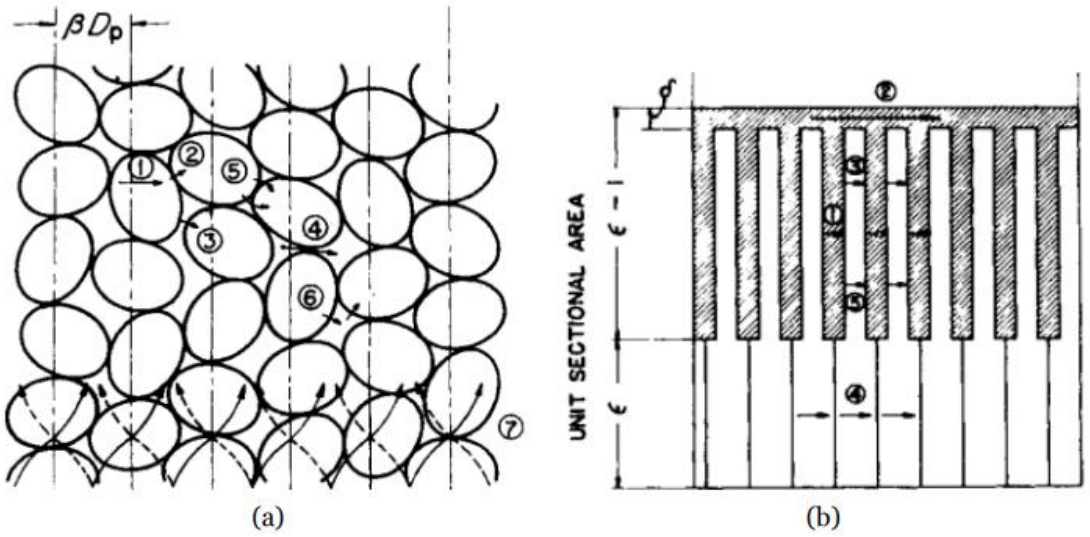

Figure 2.4: Unit cell and resistance representations (a) the Yagi-Kunii unit cell, (b) Yagi-Kunii resistances (Yagi & Kunii, 1957).

The YK model describes heat transfer occurring through simultaneous pathways. The top pathway represents heat conduction via direct particle contact following mechanism 2. The core pathway combines various mechanisms: solid conduction by mechanism 1, surface radiation by mechanism 3, and fluid-film conduction by mechanism 5, where mechanisms 1 and 5 are connected in series alongside mechanism 3. The lower pathway accounts for heat transfer through empty spaces by mechanism 4 (Botterill et al., 1989; Yagi & Kunii, 1957). Utilizing electrical resistance analogies and simplifying leads to the following correlation:

$$k_e = k_f \left(\epsilon \frac{\beta \cdot d_p \cdot h_{rv}}{k_f} + \frac{\beta(1-\epsilon)}{\gamma\left(\frac{k_f}{k_s}\right) + \frac{1}{\frac{1}{\Phi} + \frac{d_p \cdot h_{rs}}{k_f}}} \right) \qquad \text{Eq. 2.3}$$

Also, $h_{rs} = \frac{0.1952\psi}{2-\psi} \cdot \left(\frac{T}{100}\right)^3$

and $h_{rv} = 0.1952 \left(1 + \frac{\epsilon(1-\psi)}{2\psi(1-\epsilon)}\right)^{-1} \cdot \left(\frac{T}{100}\right)^3$

Where δ represents the contact area ratio between adjacent particles, β describes the geometric arrangement of particles within the bed, h_{rv} quantifies radiation through empty spaces, and h_{rs} evaluates radiation between solid materials. These parameters collectively govern the thermal resistance network in the granular system.

The equation consists of three key terms, each representing a different heat transfer mechanism, including: (1) conduction via contact surfaces, (2) the solid-void conduction within the mixture, and (3) radiation between void spaces. Under atmospheric conditions below 400°C, the effects of contact conduction and radiation are minimal and can be ignored. Since the exact contact parameters are unknown, the first term is omitted, and rest are set to $\gamma = 2/3$ and $\beta = 0.9$, as recommended by (Qian et al., 2018).

Kunii-Smith Model

An extension of the Yagi-Kunii model, the Kunii-Smith framework simplifies analysis to two parallel paths instead of three. This simplified approach merges conduction through particle contact points facilitated through conduction via a surrounding thin fluid layer and solid-surface radiation into a single parallel path. A key advancement is the incorporation of convective heat transfer occurring through voids, connected in sequence with void-to-void radiation (Kunii & Smith, 1960). Though contact area effects are negligible, void convection markedly increases ETC predictions. Both models assume spherical particles with minimal contacts.

$$k_e = k_f \left(\epsilon \left(1 + \frac{\beta \cdot h_{rv} \cdot d_p}{k_f} \right) + \frac{\beta(1-\epsilon)}{\gamma\left(\frac{k_f}{k_s}\right) + \frac{1}{\frac{1}{\phi} + \frac{d_p \cdot h_{rs}}{k_f}}} \right) \qquad \text{Eq. 2.4}$$

Where the radiative coefficient for void spaces $h_{rv,}$ and the radiative coefficient for solid surfaces h_{rs}

$$h_{rv} = 0.227 \left(1 + \frac{\epsilon(1-\psi)}{2\psi(1-\epsilon)} \right)^{-1} \cdot \left(\frac{T}{100} \right)^3$$

and $\quad h_{rs} = \frac{0.227\psi}{2-\psi} \cdot \left(\frac{T}{100} \right)^3$

Among all parameters, ϕ is particularly difficult to assess as it represents the apparent thickness of the fluid layer surrounding particle contact points.

Packed beds can be fundamentally characterized by two packing configurations: (1) a loose state (φ_1, with coordination number $n_1 = 1.5$ and void fraction $\varepsilon_1 = 0.476$) and (2)

a dense state (φ_2, where n_2 = 4/3 and ε_2 = 0.26). Given a particulate system with quantified void fraction, φ can be expressed through:

$$\phi = \phi_2 + (\phi_1 + \phi_2)\frac{\epsilon - 0.26}{0.216} \quad \text{for } 0.26 \leq \epsilon \leq 0.476$$

Zehner (ZS & ZBS) Models

According to the Zehner-Schlünder (ZS) model, as in Figure 2.7.4a, a unit cell is represented by two coaxial cylinders, where the outer region is fluid-only and the inner region contains a combination of solid and fluid. The solid phase geometry within the inner cylinder is characterized by a shape factor "B" as of the authors. Heat transfer occurs through parallel pathways in both cylinders, with the inner cylinder's solid and fluid phases exhibiting series thermal resistance. The model creates a relationship between the outer cylinder's radius and medium porosity with empirical data (Hsu et al., 1994).

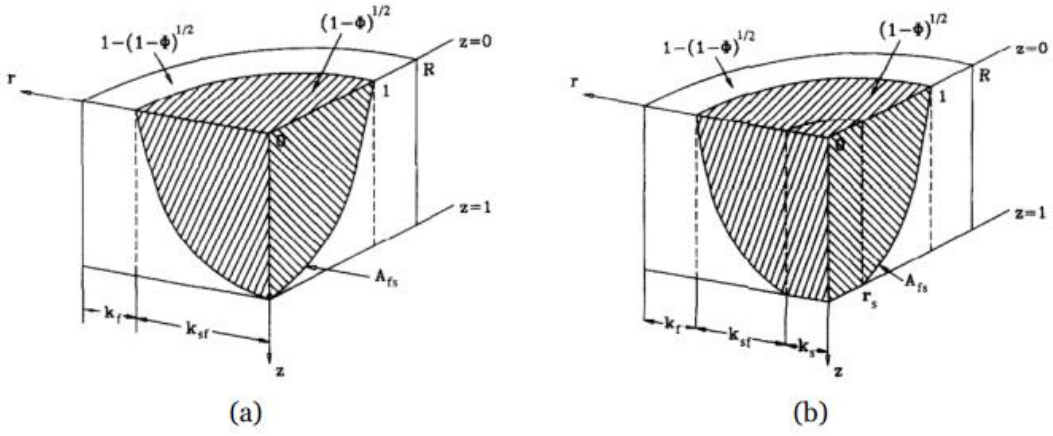

Figure 2.5: Zehner Modal unit cell representation, (a) The Zehner-Schlünder unit cell, (b) Zehner-Bauer model unit cell (Hsu et al., 1994).

Introducing a contact factor, as in Fig. 2.7.4b, refines the model by accounting for finite particle contact. This modification yields marginally higher thermal conductivity predictions, especially for systems with high solid-to-fluid conductivity ratios ($k_s/k_f > 10^3$). The enhanced formulation considers three parallel routes: (1) conduction through the outer fluid annulus, (2) combined solid-fluid conduction in the intermediate cylinder, and (3) pure solid conduction in the central core. The incorporation of contact

area terms transforms the original Zehner-Schlünder model into what is now designated as the Zehner-Bauer (ZB) model (Qian et al., 2018).

Sih et al. further enhanced the Zehner-Schlünder framework through the integration of a radiative heat transfer component originally developed by Damköhler (Sih & Barlow, n.d.). The Zehner-Damköhler correlation represents an enhanced formulation that incorporates radiative heat transfer effects in both cylindrical components of the unit cell, consolidating these contributions into a unified expression $k_e^{tot} = k_e^c + k_e^r$, where with k_e^c being the correlated effective conductivity and k_e^r the radiative contribution.

The Zehner approach utilizes parameter B to quantify deformation effects, specifying how the solid phase is geometrically structured inside a unit cell's particle arrangement.

$$B = 1.25\left(\frac{1-\epsilon}{\epsilon}\right)^{10/9} \qquad \text{Eq. 2.5}$$

The enhanced Zehner-Bauer model incorporates two important refinements. First, it accounts for pressure dependence, which is determined by the bed's Knudsen number (K_n), calculated as the ratio of gas molecule mean free path to characteristic pore dimension. At higher K_n values, the conductivity of the gas phase becomes sensitive to pressure changes. Second, it includes radiative transfer effects, represented by the Damköhler-derived radiative conductivity (k_r), which captures the impact of thermal radiation.

$$k_r = 4\sigma F d_p T^3 \qquad \text{Eq. 2.6}$$

The parameters in this formulation include: the Stefan-Boltzmann constant (σ), which governs radiative heat transfer; the radiation exchange factor (F), representing the efficiency of thermal radiation exchange between surfaces; the average particle diameter (d_p) measured in meters; and the absolute temperature (T) in Kelvin.

Similar to the diverse mathematical representations for ETC, multiple definitions exist for the radiation exchange factor (F) as characterized by Qian et al. This study comparatively assesses three prominent F formulations, outlined as in Table 2.1.

Table 2.1: Radiation exchange factors (Qian et al., 2018)

Authors	Radiation Exchange Factor, F
Wakao	$F_W = \frac{2}{2/\psi - 0.264}$
Zehner Schlünder	$F_Z = \frac{\left(1-\sqrt{1-\mathrm{k}_f}\right)\mathrm{k}_f}{2/\psi - 1} + \frac{\sqrt{1-k_f}}{2/\psi - 1} \cdot \frac{B+1}{B} \cdot \frac{1}{1+\frac{1}{(2/\psi - 1)\Lambda}}$
Breitbach Barthels	$F_B = \left(1-\sqrt{1 \quad -\mathrm{k}_f}\right)\mathrm{k}_f + \frac{\sqrt{1-k_f}}{2/\psi - 1} \cdot \frac{B+1}{B} \cdot \frac{1}{1+\frac{1}{(2/\psi - 1)\Lambda}}$

Table 2.1 illustrates that radiative conductivity is influenced by several factors, including the deformation factor, porosity, particle emissivity, particle diameter, and temperature. When the deformation factor is considered through Equation 3.6 and an emissivity value of 0.7 is assumed, the three-radiation exchange factor (F) formulations yield nearly identical ETC predictions. However, at higher emissivity and deformation factor values, discrepancies between the equations emerge, underscoring the sensitivity of radiative heat transfer to these parameters. For modeling accuracy, this study adopts the Breitbach-Barthels formulation for F, validated as the most reliable across diverse conditions. Unlike simpler alternatives that only consider intra-cell radiation, this comprehensive formulation accounts for (Qian et al., 2018).

The Zehner-Bauer model accounts for particle contact area effects through a contact parameter (ω). While Qian et al. established an empirical value of ω = 0.0072 for ceramic spheres, Tsotsas and Martin recommend ω = 0.0010 for fractured sand grains - the material system examined in this work (Tsotsas & Martin, 1987). We evaluate two model implementations: with and without the contact term. Results demonstrate that accounting for the contact area produces minimal influence on effective thermal conductivity (ETC) calculation when using the sand-specific ω value of 0.0010.

Due to limited data on precise data regarding sand's shape factor, granular size spreading, and Knudsen number for this system, we adopt a reduced-complexity formulation of the Zehner -Bauer (ZB) model that omits these parameters. The complete model formulation, including all terms, is thoroughly described in (Tsotsas & Martin, 1987). The simplified version implemented in this study is given by:

$$k_e^{ZBS} = k_f \left(\left(1 - \sqrt{1-\epsilon}\right) + \sqrt{1-\epsilon} \cdot (\omega\kappa + (1-\omega)\Gamma) \right) \quad \text{Eq. 2.7}$$

And,

$$\Gamma = \frac{2}{1-\frac{B}{\kappa}} \left(\frac{\kappa-1}{\left(1-\frac{B}{\kappa}\right)^2} \frac{B}{\kappa} \cdot ln\left(\frac{\kappa}{B}\right) - \frac{B-1}{1-\frac{B}{\kappa}} - \frac{1}{2}(B+1) \right) \quad \text{Eq. 2.8}$$

Tables 2.2: The Kunii and Zehner model equations, enhanced with Damhöhler's radiative transfer terms.

Correlation	ETC Representation
Yagi -Kunii(YK) with radiation (Yagi & Kunii, 1957)	$k_e^{YK,r} = k_f \left(\epsilon \frac{\beta \cdot d_p \cdot h_{rv}}{k_f} + \frac{\beta(1-\epsilon)}{\gamma\left(\frac{k_f}{k_s}\right) + \frac{1}{\frac{1}{\phi} + \frac{d_p \cdot h_{rs}}{k_f}}} \right)$ $h_{rv} = 0.1952 \left(1 + \frac{\epsilon(1-\psi)}{2\psi(1-\epsilon)}\right)^{-1} \cdot \left(\frac{T}{100}\right)^3$ $h_{rs} = \frac{0.1952\psi}{2-\psi} \cdot \left(\frac{T}{100}\right)^3$
Kunii-Smith with radiation (Kunii & Smith, 1960)	$k_e^{KS,r} = k_f \left(\epsilon \left(1 + \frac{\beta \cdot h_{rv} \cdot d_p}{k_f}\right) + \frac{\beta(1-\epsilon)}{\gamma\left(\frac{k_f}{k_s}\right) + \frac{1}{\frac{1}{\phi} + \frac{d_p \cdot h_{rs}}{k_f}}} \right)$ $h_{rv} = 0.227 \left(1 + \frac{\epsilon(1-\psi)}{2\psi(1-\epsilon)}\right)^{-1} \cdot \left(\frac{T}{100}\right)^3$ $h_{rs} = \frac{0.227\psi}{2-\psi} \cdot \left(\frac{T}{100}\right)^3$
Zehner-Schlünder (ZS)	$k_e^{ZS} = k_f \left(\left(1 - \sqrt{1-\epsilon}\right) + \sqrt{1-\epsilon} \cdot \Gamma \right)$ $\Gamma = \frac{2}{1-\frac{B}{\kappa}} \left(\frac{\kappa - 1}{\left(1-\frac{B}{\kappa}\right)^2} \frac{B}{\kappa} \cdot ln\left(\frac{\kappa}{B}\right) - \frac{B-1}{1-\frac{B}{\kappa}} - \frac{1}{2}(B+1) \right)$
Zehner-Bauer-Schlünder (ZBS)	$k_e^{ZBS} = k_f \left(\left(1 - \sqrt{1-\epsilon}\right) + \sqrt{1-\epsilon} \cdot (\omega\kappa + (1-\omega)\Gamma) \right)$
Zehner-Schlünder with radiation (Qian et al., 2018)	$k_e^{ZS,r} = k_e^{ZS} + k_e^r$ and $k_e^r = 4F_B \sigma d_p T^3$ $F_B = \left(1 - \sqrt{1-\epsilon}\right)\epsilon + \frac{\sqrt{1-\epsilon}}{2/\psi - 1} \cdot \frac{B+1}{B} \cdot \frac{1}{1 + \frac{1}{(2/\psi - 1)\Lambda}}$
ZBS with radiation (Qian et al., 2018)	$k_e^{ZBS,r} = k_e^{ZBS} + k_e^r$

Table 2.3: The functional forms used in the ETC correlations.

Parameter	Expression	Descriptions
κ	$\frac{k_s}{k_f}$	The relative thermal conductivity of solid versus fluid components
Λ	$\frac{k_s}{4\sigma d_p T^3}$	Term simplification (Qian et al., 2018)
ϕ	$\phi = \phi_2 + (\phi_1 + \phi_2)\frac{\epsilon - 0.26}{0.216}$ for $0.26 \leq \epsilon \leq 0.476$ $\phi = \phi_1$ for $\epsilon \geq 0.476$ And $\phi = \phi_2$ for $\epsilon \leq 0.26$ $\phi_{1or2} = \frac{0.5\left((\kappa - 1)/\kappa\right)^2 \cdot sin^2(\theta_0)}{ln\left(\kappa - (\kappa - 1)\ cos(\theta_0)\right) - \left((\kappa - 1)/\kappa\right)\left(1 - cos(\theta_0)\right)} - \frac{2}{3\kappa}$ $sin^2(\theta_0) = 2/3$ for $\epsilon \geq 0.476$ $sin^2(\theta_0) = 1/\left(4\sqrt{3}\right)$ for $\epsilon \leq 0.26$	fitting parameter that represents the fluid film thickness surrounding granular material (Kunii & Smith, 1960)
ϵ	$\epsilon = 1 - \frac{\rho_{bulk}}{\rho_{grain}}$	the porous volume fraction within the sand bed
k_s	$0.95 + 1.21 \cdot 10^{-3} \cdot T + 7.19 \cdot 10^{-7} \cdot T^2$	TES grain thermal conductivity W/(m.K) (COMSOL)
B	$1.25\ \left(\frac{1-\epsilon}{\epsilon}\right)^{10/9}$	Deformation parameter (Qian et al., 2018)
ρ_{bulk}	1425	Bulk density of the sand kg/m^3(*Quartz*, n.d.)
ρ_{grain}	2650	Density of a sand grain kg/m^3(*Quartz*, n.d.)
ψ	0.7	Sand Emissivity
d_p	0.5	Average grain size (mm)(Qian et al., 2018)
k_f	$6 \cdot 10^{-5} \cdot T + 0.0081$	TES air thermal conductivity W/(m.K) (COMSOL)
β	0.9	Deformation parameter ((Yagi & Kunii, 1957))
γ	2/3	Fitting parameter ((Yagi & Kunii, 1957))
ω	0.0010	Contact surface parameter ((Hsu et al., 1994))
σ	$5.67 \cdot 10^{-8}\ \mathrm{W}/(m^2 \cdot K^4)$	Stefan-Boltzmann constant

2.5 Characterization of ETC in Granular Medium

Díaz-Heras *et al*. highlighted limitations of the Kunii-Smith model for the ETC in packed beds, particularly its tendency to underestimate stagnant thermal conductivity compared to experimental data. In contrast, the Zehner-Schlünder correlations show a much closer match with real-world measurements, especially when the thermal conductivity ratio of solid to fluid phases (k_s/k_f) ranges from 10 to 200 (Díaz-Heras et al., 2020). While most studies reviewed focused on large-particle systems like ball bearings and glass beads, Tavman's study extended the Zehner-Schlünder model to finer granular materials such as sand (grain size: 0.85–1.18 mm; porosity: 0.215–0.476) (Tavman, 1996). Though the model slightly underpredicted ETC for smaller grains, it remained largely valid. The review also concludes that radiative heat transfer has minimal impact at temperatures below 900°C (Díaz-Heras et al., 2020).

The fluid phase's thermal conductivity significantly influences the system's effective thermal conductivity (ETC). For the temperature range relevant to this TES study, air's thermal conductivity exhibits substantial variation (Hamdhan & Clarke, 2010; Kadoya et al., 1985), rendering the ETC inherently temperature-dependent. Research by Hamdhan et al. demonstrates that while standard reference values suffice at ambient conditions, they systematically underpredict thermal conductivity at elevated temperatures (Hamdhan & Clarke, 2010). This temperature dependence necessitates particular attention, as the TES's ETC will show a measurable increase with rising operational temperatures.

Through a comprehensive analysis of experimental thermal conductivity data across multiple materials and temperature ranges, Tsotsas and Martin demonstrate a consistent positive correlation between particle size and effective thermal conductivity (ETC). Their findings reveal that larger mean particle diameters amplify radiative heat transfer contributions, with this effect growing progressively more pronounced at elevated temperatures (Tsotsas & Martin, 1987).

Botterill et al. analyzed seven different ETC models and found that none could fully capture the strong temperature dependence above 350°C. Their study showed that unit-cell models tend to overlook long-range radiation effects, leading to underestimations

at higher temperatures (350–900°C). One key factor behind this discrepancy is sand's high optical transmittance (0.54), which increases as temperature rises, resulting in experimental ETC values that exceed model predictions. Accuracy improved when models incorporated temperature-dependent transmittance effects (Botterill et al., 1989).

Qian et al. examine various ETC models and their suitability for CFD simulations, finding that the Zehner-Bauer (ZB) model, when accounting for a radiative contribution ($k_e^{tot} = k_e^{ZB} + k_e^r$), closely matches experimental results under diverse conditions. Their analysis, conducted with three distinct mean particle diameters, showed that for particles smaller than 0.5 mm, the radiative component of thermal conductivity has minimal impact at temperatures below 1000°C. This suggests that radiation plays an insignificant role in overall heat transfer for finer particles (Qian et al., 2018).

Although several methodologies have been formulated to calculate ETC in particle beds, all show some discrepancy when compared to empirical results. By systematically comparing experimental results, this study aims to identify the correlation that best predicts temperature distributions in packed beds.

2.6 Examples of Packed Bed Models

Researchers have developed various 3D packed bed models with different levels of complexity. For example, Mahfoudi et al. demonstrate a streamlined COMSOL-based modelling to conduct a simplified study on sensible heat storage in sand. Although their paper provides few details about the model's construction, this approach implies treatment of the sand as a uniform solid having consistent thermal conductivity, with heat transfer limited to conduction between the sand and working fluid (Mahfoudi et al., 2014).

Laubscher et al. created a 2D CFD model using ANSYS Fluent to analyze a TES system utilizing packed rock beds, where forced air was used as the HTF. This initial study aimed to provide qualitative insights before conducting experimental tests. The model represented the rock pile as a permeable medium having 0.45 porosity, with airflow dynamics calculated using the k−ϵ turbulent flow model. The results played a key role

in optimizing the design by identifying critical areas that required better insulation (Laubscher et al., 2017).

Zavattoni et al. created a computational model of a pebble-filled TES system encased in concrete, employing forced air convection for heat transfer. This approach was based on the Kunii-Smith method for ETC but included additional terms to account for Darcian airflow through the porous medium. The study revealed that radiative heat transfer gains prominence at 300°C and dominates thermal transport beyond 500°C in their pebble-packed system (Zavattoni et al., 2012).

CHAPTER THREE: METHODOLOGY

The research procedure is segmented into four phases. Firstly, a comprehensive literature review was performed to identify existing knowledge gaps to understand the significant parameters that may negatively impact the TES system's operational efficiency when sand is used as the thermal medium. The study begins with experimental work to obtain time-dependent temperature profiles at three points within the TES system. While the full experimental design is beyond the scope of this work, an overview is provided in the following chapter. To identify the parameters influencing the system's temperature, a finite element-based three-dimensional numerical simulation was implemented to model the TES system. This process involves examining the fundamental equations governing heat transfer in solid materials, highlighting the critical role of thermal conductivity for each material. A literature review in Section 2.7 emphasizes the complexity of thermal conductivity in granular materials. The work systematically examines the effective medium approach for granular thermal conductivity, followed by an exploration of different conductivity models.

Additionally, a study is conducted to quantitatively analyze how each parameter influences the TES temperature during the charging process. By combining these approaches, the study characterizes the parameters affecting TES temperature, identifies accurate modeling techniques, and evaluates ETC correlations. Ultimately, the developed model serves as an exploratory research tool for optimizing the TES system design.

3.1 The Finite Element Method

This model aims to predict time-based temperature evolution across the entire system, enabling investigation of thermal behavior under design variations. Solving the heat equation (as shown in Equation 2) is essential for determining transient temperature distributions and corresponding heat fluxes.

Considering both the nonlinear phenomena and intricate geometry of the system, finding an exact analytical solution is impractical, making numerical methods necessary. To address this, COMSOL Multiphysics was used for finite element analysis

(FEA), breaking the domain into a mesh where partial differential equations are approximated and solved through iterative calculations. This method enables a comprehensive and reliable assessment of the transient thermal behavior in the TES system.

The analysis operates on COMSOL's heat transfer module, which solves the classical heat equation with temperature as the solution variable. This approach yields comprehensive time-dependent solutions for both temperature fields and heat flux distributions throughout the computational domain.

3.2 Effective Thermal Conductivity (ETC) Models

This study assesses selected ETC models that account for radiative heat transfer, as detailed in Section 2.7, including the Yagi-Kunii (YK) model, Kunii-Smith (KS), Zehner -Schlünder (ZS), Zehner -Bauer (ZBS), and Zehner -Damköhler with radiation terms.

3.3 Research Framework

As indicated in Equation 2.2, solving the heat equation necessitates input parameters including heat source, material density, effective thermal conductivity, and specific heat capacity terms. While density and heat capacity values can be acquired from published data or experimental measurements, evaluation of thermal conductivity requires application of effective medium approximations. Consequently, the modeling approach was organized into primary and secondary components, as depicted in the methodological framework presented in Figure 3.1.

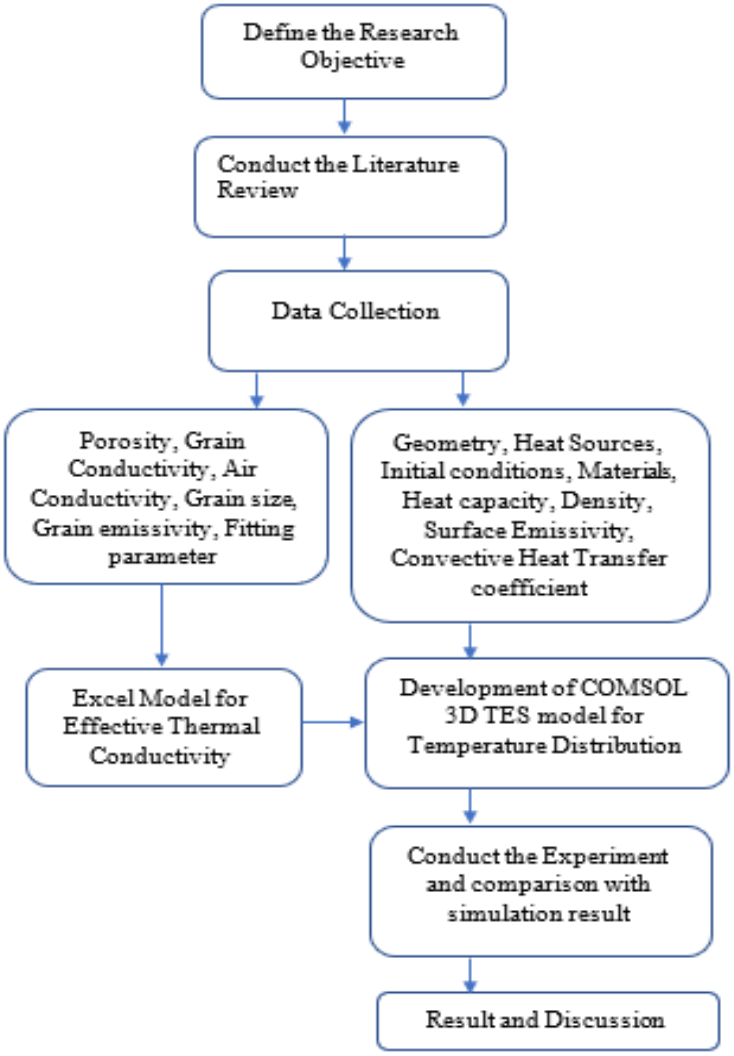

Figure 3.1: The modeling framework comprising primary and secondary components.

As depicted in Figure 3.1, the COMSOL primary model processes right-side inputs to solve the heat equation, while thermal conductivity values are generated by the Excel secondary model using left-side inputs. A secondary Excel model calculates ETC values at six different temperature points, ranging from 298 K to 773 K in specific increments, for each selected correlation. These values are then used as temperature-dependent material inputs in the COMSOL simulation. Since different ETC models produce varying thermal distributions within the TES system, the COMSOL setup includes a Material Switch feature to allow systematic comparison between them. To achieve this, the model incorporates required sand material definitions, each representing a different thermal conductivity formulation.

3.4 Excel Model for Effective Thermal Conductivity

The mathematical formulations for all ETC correlations covered in Section 2.4—including Yagi-Kunii (YK) model, Kunii-Smith (KS), Zehner-Schlünder (ZS), Zehner-Bauer (ZBS), and Zehner-Damköhler (with radiation terms)—are summarized in Table 2.2. The implementation process included three key steps: (1) creating separate User-Defined Materials for each ETC correlation, from Yagi-Kunii to Zehner-Damköhler, (2) assigning interpolated thermal conductivity functions derived from Excel data, assuming a linear variation between discrete temperature points, and (3) During simulation, performing a material sweep to analyze and compare the different ETC models effectively.

3.5 COMSOL Modeling Workflow for the Heat Transfer Analysis

3.5.1 Geometry Definition in the COMSOL

The modeling process began with geometry preparation, where the TES system's CAD model was imported into COMSOL. To enable temperature monitoring and model validation, four specific points were added in the 3D model at the locations corresponding to experimental thermocouples. These reference points serve as monitoring stations for thermal analysis, allowing direct comparison between simulated and empirical results. The placement of these probe points within the overall geometry is illustrated in Figure 3.2.

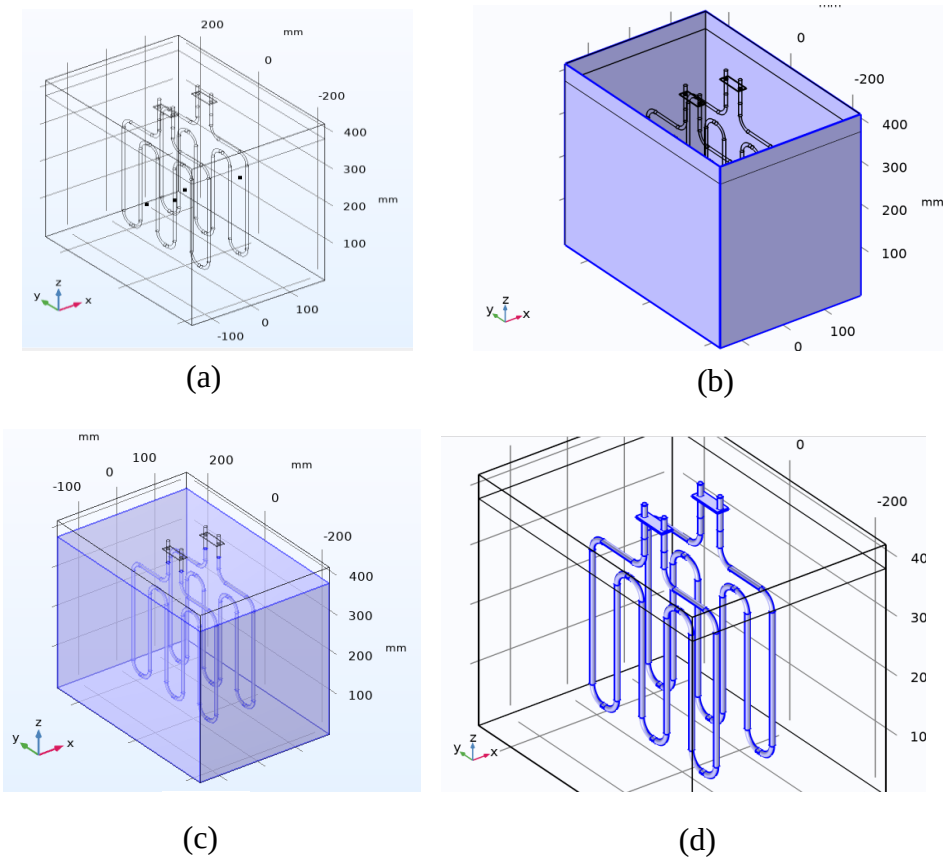

Figure 3.2: Complete TES model system layout, (a) Full geometry of TES system, (b) TES container, (c) TES material reservoir, and (d) Heating elements.

3.5.2 Materials Assignments

After defining the geometry, the next step involves assigning material properties to the various material domains and interfacial boundaries of the 3D model representing the TES system. This step is crucial in COMSOL because accurately selecting a domain and defining material properties ensures the model reflects real-world behavior and directly impacts the reliability and accuracy of the results.

3.5.3 Container

The aluminum container structure enclosing the thermal storage medium is defined by properties outlined in Table 3.1.

Table 3.1: Container Parameter

Parameter	Numerical Value	Units	Data Source
Heat capacity	900	J/(kg· K)	COMSOL Material Library
Surface emissivity	0.1	—	(*Surface Emissivity Coefficients.*, n.d.)
Thermal conductivity	238	W/(m·K)	COMSOL Material Library
Density	2700	kg/ m^3	COMSOL Material Library

3.5.4 Heating Element

The heaters are modeled based on an initial examination of tubular resistance heater designs. The heating units comprise zinc-alloy resistance coils embedded in dense magnesium oxide (MgO) powder, which provides electrical insulation while facilitating heat transfer to the surrounding Inconel 800 alloy casing. A detailed heater model could be developed using COMSOL Multiphysics' electrical currents module, incorporating a complex geometry. Although applying voltage to the resistance wire could precisely replicate experimental power dissipation, the necessary multiphysics modeling is beyond the scope of this study. Instead, a simplified approach was used, representing the heater as an MgO volume encased in Inconel 800, with a uniform heat generation of 2000 W, based on manufacturer specifications. The material properties are detailed in Table 3.2.

Table 3.2: Heating Element Parameter

Component	Parameter	Numerical Value	Units	Data Source
Magnesium Oxide (MgO)	Density	3500	kg/m^3	COMSOL Material Library
MgO	Thermal conductivity	$0.99 + 3.68E-4 \cdot T + 5.86E-8 \cdot T^2$	W/(m·K)	COMSOL Material Library
MgO	Heat capacity	877	J/(kg·K)	(*Magnesium Oxide MgO Optical Material | Crystran*, n.d.)
Inconel 800	Surface emissivity	0.2	—	(*Emissivities*, n.d.)

3.5.5 TES Material

The thermal storage medium in this investigation is implemented as a custom-defined material within the simulation environment. To ensure the model functions correctly, key inherent material characteristics comprising heat capacity per unit mass, thermal conductivity, and volumetric density are required. The heat capacity (c_p) and mass density (ρ), and parameters for the granular sand material can vary to some extent based on factors such as types of minerals present, porosity, grain diameter, and moisture concentration, which may differ depending on its geographical origin. However, in the case of dry sand, the variation is not drastic, and it is generally within a predictable range. Therefore, the selected secondary data for the heat capacity of sand is utilized from various literature sources, with the reported values presented in Table 3.3.

ETC values were calculated in Excel using multiple correlation models, requiring separate TES material definitions to account for variations in conductivity, particularly at higher temperatures where radiation effects become significant. To incorporate this variability into the COMSOL model, a "Material Switch" node is implemented, allowing the simulation to run for each material and systematically evaluate ETC correlations.

Table 3.3: Parameters used to define the sand-packed-bed TES material.

Material Property	Value	Unit	Source
Bulk density of the sand (ρ_{bulk})	1425	kg/m³	(Ižvolt & Dobeš, 2014; Qian et al., 2018; *Specific Heat of Common Substances*, n.d.)
Sand specific heat capacity	T [K]	Cp [J/(kg·K)]	
	333	776	
	373	827	
	473	936	
	573	1009	
	673	1072	
	773	1133	
Sand surface emissivity	0.7	—	(Qian et al., 2018)

3.5.6 COMSOL Physics

The simulation framework incorporates COMSOL's specialized Heat Transfer in Solids physics interface for modeling thermal behavior. The fundamental heat transfer equation governing this process is expressed as:

$$\rho C_p \frac{\delta T}{\delta t} - k\nabla^2 T = Q \qquad \text{Eq. 2.2 revisited}$$

heat equation incorporates: T (temperature, K), ρ (density, kg/m³), Q (heat source, W/m³), Cp (heat capacity, J/(kg·K)), k (thermal conductivity, W/(m·K)), and t (time, s) to describe the storage medium's thermal behavior.

Initial conditions set all material domains to 298K (25°C). To replicate experimental conditions, the base surface of the aluminum enclosure is modeled with an insulated boundary condition, with radiative boundary conditions (Surface-to-Ambient) implemented on all air-exposed surfaces as per:

$$-\hat{n} \cdot \hat{q} = \varepsilon\sigma (T_{amb}^4 - T^4) \qquad \text{Eq. 3.1}$$

Where n̂ (surface normal vector), q̂ (thermal flux in W/m²), and ε (surface emissivity). Radiation terms employ σ (Stefan-Boltzmann constant) and T_{amb} (ambient temperature in Kelvin)

Further, a convective boundary condition is implemented using a steady 5 W/(m²·K) air convection coefficient across all surfaces. The governing equation for this process is expressed as:

$$-\hat{n} \cdot \hat{q} = h\,(T_{amb} - T) \qquad \text{Eq. 3.2}$$

Where, h represents convective heat transfer coefficient in W/(m^2.K)

To accurately replicate the laboratory setup, heaters are modeled as controlled thermal sources. Their operation follows a control logic if-statement similar to a PID controller: if the heater thermocouple-recorded temperature falls under 500°C, the heater turns on, supplying a constant 2 KW of heat. Once the temperature reaches or exceeds 500°C, the heater switches off (0 W output). This approach ensures the simulation accurately replicates the experimental control system.

3.5.7 COMSOL Mesh and Time-steps

The final step in the FEM involves generating a COMSOL-defined mesh with normal resolution, consisting of approximately around 3116142 domain elements as shown in Figure 3.3. The model runs over a 5-hour time range with 0.1-hour steps, taking about 2 hours 51 minutes to complete on an Intel Core i7-based workstation with 16 GB memory capacity.

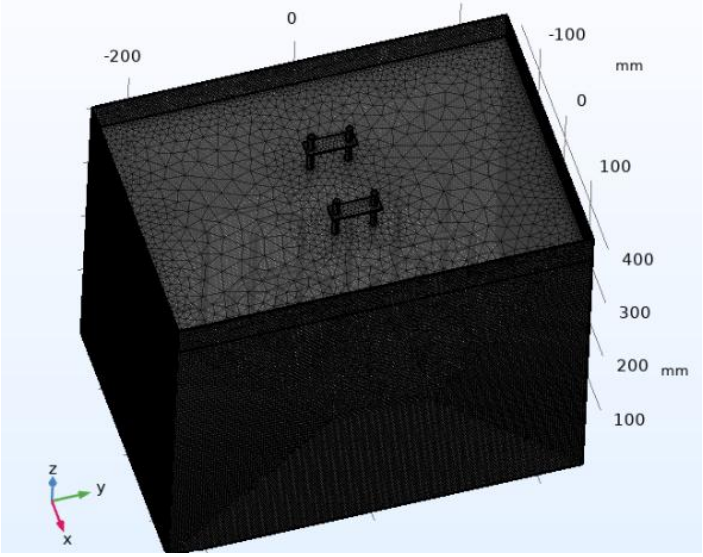

Figure 3.3: Conventional tetrahedral elements meshed using COMSOL.

3.6 Design & Experimental Setup

An experimental sand-based TES system was constructed to investigate sand's thermal heat transfer behavior. The apparatus features an aluminum containment vessel (500 × 405 × 420 mm³ internal dimensions) partially filled to 380 mm depth with dry silica sand over a plywood base layer. Two centrally positioned tubular resistance heaters (2000 W each, 360 × 290 × 50 mm³) maintain operational temperature through PID control, spaced 95 mm apart with K-type thermocouples monitoring: (1) direct heater contacts points (500°C setpoint), (2) inter-heater midpoints, (3) near heater-wall interfaces, and (4) near wall-heater interfaces. As shown in Figure 3.4b, the upper sand surface remains exposed to ambient conditions, enabling natural convection heat transfer at the upper boundary.

To achieve greater thermal diffusivity in the sand storage medium by improving ETC, we conducted a series of experiments by gradually introducing crushed stone and gravel aggregates, commonly used in construction to the sand. For this conductivity improvement experiment, the sand was layered with aggregates, and the experiment was conducted to observe the impact. Next, we mixed the aggregates uniformly with the sand and performed another round of testing. Finally, the uniformly mixed sand-

aggregate combination was layered with mixed metal chips, and the experiment was repeated, as shown in Figure 3.4c.

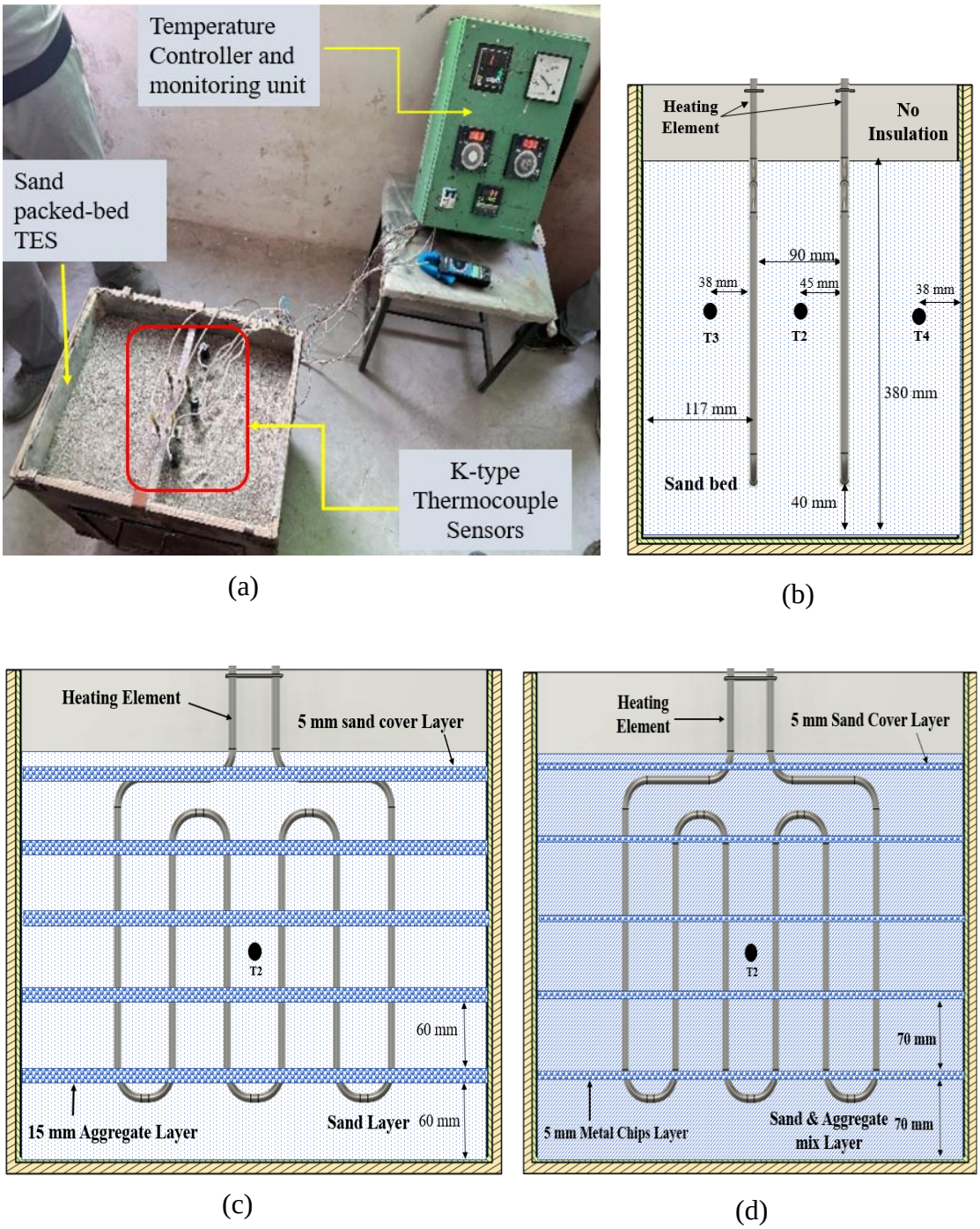

Figure. 3.4. TES experimental arrangements, (a) Overall system photograph, (b) Schematic cross-section of pure sand reference case with thermal component placement, (c) Stratified sand-aggregate mixture design, (d) Enhanced sand-aggregate-iron chip composite structure.

This investigation employed three primary materials: silica sand, crushed stone/gravel aggregates, and mixed metal chips as in Figure 3.5. The thermophysical properties of these components are characterized below:

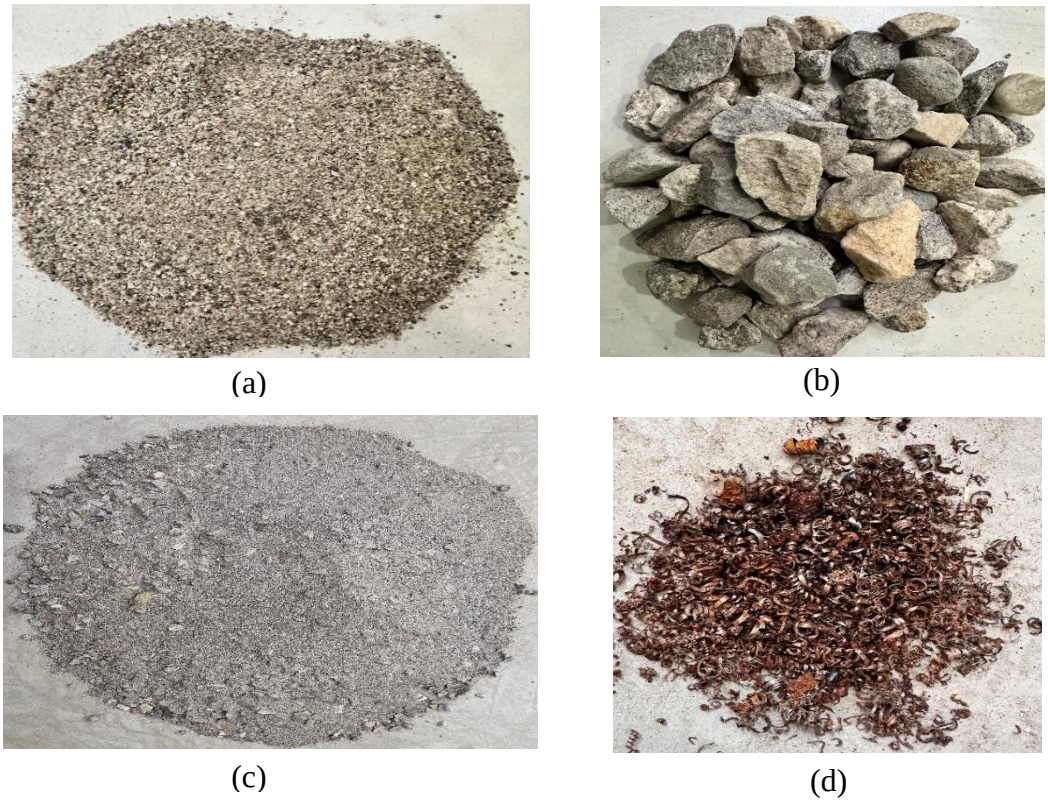

(a) (b)

(c) (d)

Figure 3.5: TES material sample, (a) Silica sand, (b) Aggregates, (c) sand aggregate uniform mixture, and (d) Scrap cast iron metal chips.

Silica sand is primarily composed of silica (SiO2) and is recognizable by its grey color (see Figure 3.5a). Its grain size ranges from 0.06 to 0.2 mm. The sand possesses bulk density of 1500 kg/m³, melting point around 1577°C, thermal conductivity ranging varies between 0.2 to 0.7 W/(m·K), and demonstrates a specific heat capacity of 830 J/(kg·K) (*Material-Properties.Org*, n.d.).

Aggregates used in construction are sourced from natural materials such as gravel and crushed stone. These aggregates can vary in size, from fine sand particle sizes (0.15 mm) to larger gravel (up to 40 mm). Their thermophysical properties depend on mineral composition and particle size. For instance, gravel and crushed stone from rocks like granite and basalt possess superior thermal conductivity relative to fine sand. Aggregates demonstrate thermal conductivity values spanning 0.2 to 1.5 W/(m· K),

during which the heat capacity typically falls between 500 and 1000 J/(kg·K). The bulk density of aggregates used in construction typically ranges from 1600 kg/m³ to 2200 kg/m³ (Howlader et al., 2012).

Cast iron metal chips, a by-product of lathe machining processes, are primarily composed of an iron-carbon alloy, which may also include silicon, manganese, and other elements. These chips are typically small, irregularly shaped pieces, with sizes varying between 0.50 mm to 5 mm. The combination of high density (6800–7500 kg/m³) and conductivity (50–70 W/(m·K)) makes cast iron ideal for heat retention in industrial furnaces. Unlike steel, cast iron's broader melting range (1150–1200°C) arises from its higher carbon content (2–4%), which also influences its thermal conductivity (50–70 W/(m·K)) (*Material-Properties.Org*, n.d.).

To address the low intrinsic thermal conductivity of sand, composite beds were created by mixing sand with materials exhibiting higher conductivity values. The experimental study was carried out with both stratified (layered) and homogeneous (uniform) configurations, with quantitative comparisons provided in Table 3.4. In the second layered method, sand and aggregate were packed in layers so that aggregate made up 24% of the total volume, as shown in Figure 3.4c. In the third uniform method, the sand and aggregate mixture was fully blended, ensuring no changes in composition. In the final layered setup, cast iron chips were placed in discrete layers, constituting 7.8% of the entire volume in the sand-aggregate mixture as in Figure 3.4d. Additionally, the metal chip layers are directly in contact with the electric heating element.

Table 3.4: Table showing the blend percentages (based on volume) of sand for the two composite preparation strategies

Materials sample composition	stratified (layered) mix	Homogeneous (uniform) mix
Silica Sand	-	-
Aggregate mixed with sand	24.5% by volume	24.5% by volume
Mixed-metallic chips mixed with the sand aggregate mixture	7.8% by volume	-

CHAPTER FOUR: RESULTS AND DISCUSSIONS

This chapter details the outcomes of computational modeling aimed at gaining a deeper understanding of heat conduction in the packed sand bed. Additionally, Experimental measurements are included to verify the computational models, along with proposed strategies for improving sand's thermal conductivity.

4.1 Experimental Results: Temperature Profiles of the Thermocouples

Heater surfaces reached and maintained the 500°C operational temperature within 30 minutes, as evidenced in Figure 4.1, and remained stable throughout the sustained heating operation, suggesting efficient heating with effective temperature control but heat diffusion into the sand is relatively slow, as nearby areas (T2, T3, T4) do not heat up as quickly.

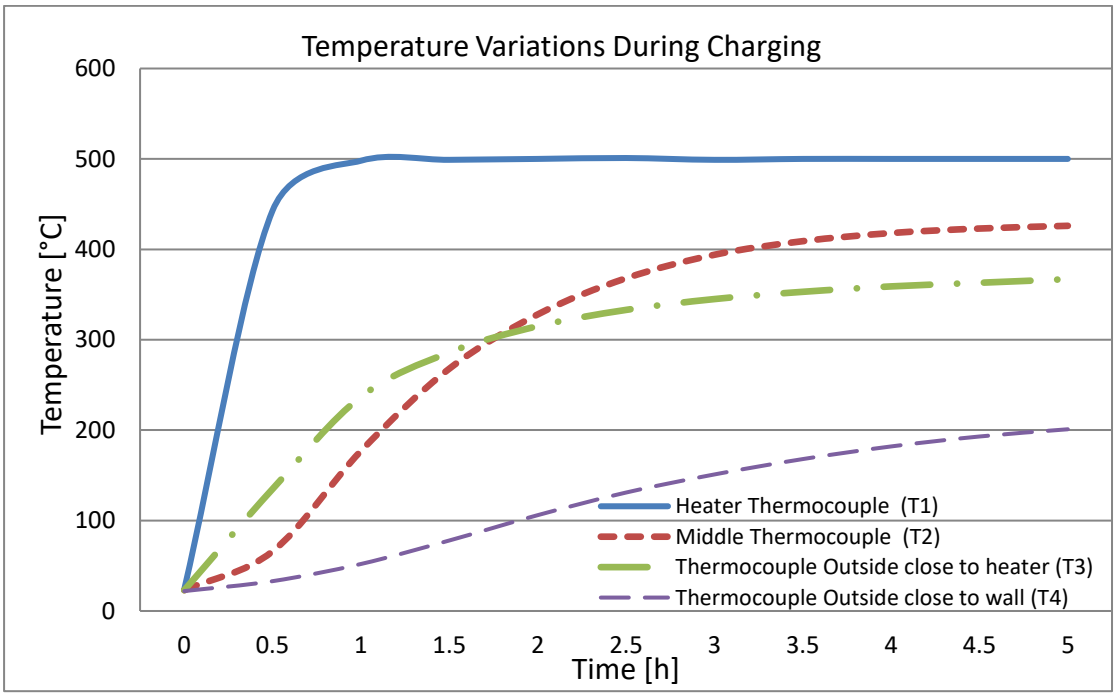

Figure 4.1: Thermocouple-recorded temperature data collected at distinct positions over a five-hour experimental duration.

Initially, near the heater but outside the main heating zone, the temperature at T3 rises significantly, reaching 237°C in 1 hour and later 367°C in 5 hours, but remains lower than the midpoint T2, which is located between the heater and the wall. Heat flows primarily through the sand by conduction, with limited additional radiation coming

from the heater, making it slower yet effective. The midpoint T2 heats up slowly due to gradual conduction through sand, reaching 177°C in 1 hour, and the temperature increase slows down after 3 hours, stabilizing around 426°C at 5 hours. Sand's thermal inertia causes a delayed temperature rise, creating a steady-state temperature gradient, but full thermal equilibrium has not yet been reached in 5 hours. The temperature at T4 region 38 mm near the wall rises slowly, reaching only 201°C in 5 hours, with a much lower temperature gradient than T2 and T3. This difference is because the T4 region experiences different system boundaries exhibiting substantial environmental heat losses due to a low level of insulation. Since the sandbox is not fully insulated, the temperature drops quickly in the area between the heating elements and the walls, unlike in the T2 region, where heat retention is higher. Unlike the outer boundary, where heat escapes rapidly due to direct exposure to the environment, T2 experiences different boundary conditions, allowing it to retain heat more effectively.

First, the T2 region acts as a heat trap because the heat sources present on both sides prevent heat from escaping quickly into the surroundings. Additionally, thermal lag occurs in this area because of sand's low thermal conductivity and high heat capacity, meaning it retains heat longer and cools down slowly even when the heat sources are turned off. As a result, a nearly steady-state thermal gradient establishes itself between adjacent heating elements. This understanding helps in designing TES systems using packed beds, which can maintain uniform temperature distribution without requiring a mixing mechanism. This approach improves efficiency, reduces costs, and simplifies system design by eliminating unnecessary moving parts.

Keeping this in mind, going forward, the temperatures shown in Figure 4.1 are important for future reference, as they will help model validation. Accurate temperature predictions at all four monitoring locations throughout the experimental duration would confirm the model's reliability in representing the actual TES system's behavior.

4.2 Excel-Based Calculations: ETC Trends Curves

Examination of the correlation models presented in Tables 2.2 and 2.3 identifies several key variables that are fundamental to solving all predictive equations. Using the key parameter values listed in Table 4.1, all mathematical expressions and its constituent subexpressions become solvable. These variables maintain fixed values during the evaluation of each correlation equation.

Table 4.1: Parameter values for solving all ETC correlations across temperature inputs.

Parameter	Values	Descriptions	Data Source
ρ_{bulk}	1425	Bulk density of the sand [kg/m³]	(*Quartz*, n.d.)
ρ_{grain}	2650	Density of a sand grain [kg/m³]	
$\boldsymbol{\epsilon}$	$1 - (\rho_{bulk}/\rho_{grain}) = 0.46$	Sand Porosity	Derived
k_s	$0.95 + 1.21\times10^{-30}.\ T + 7.19\times10^{-7}.\ T^2$	TES grain thermal conductivity W/(m·K)	(Shi et al., 2023)
ψ	0.7	Sand grain emissivity	(Qian et al., 2018)
d_p	0.5	Average grain size [mm]	(*Quartz*, n.d.)
k_f	$6 \times 10^{-5} \cdot T + 0.0081$	TES air thermal conductivity W/(m·K)	(Stephan & Laesecke, 1985)
$\boldsymbol{\beta}$	0.9	Deformation parameter (Yagi-Kunii; Kunii-Smith)	(Kunii & Smith, 1960; Qian et al., 2018)
γ	2/3	Fitting parameter	(Kunii & Smith, 1960; Qian et al., 2018)
ω	0.0010	Contact area parameter (Zehner models)	(Tsotsas & Martin, 1987)

Employing these parameter values, the ETC was computed at five discrete temperature points for each conductivity model. The outcomes of this analysis are illustrated in Figure 4.2.

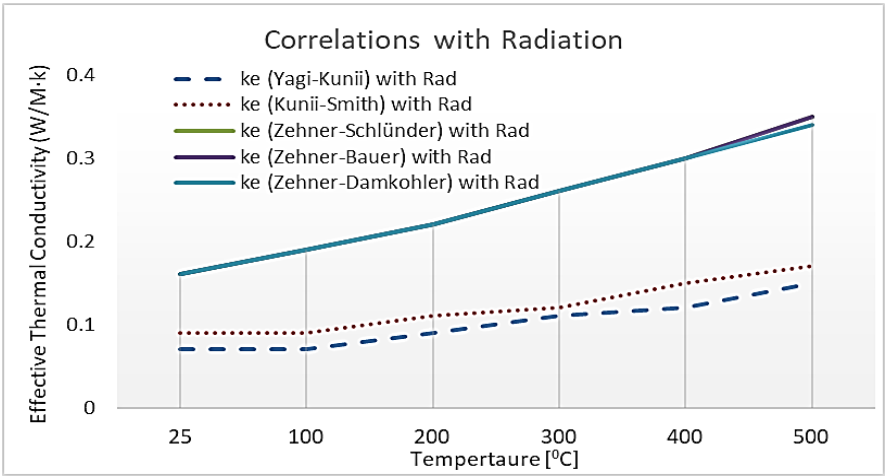

Figure 4.2: Graphical representation of the ETC correlations incorporating radiative transfer terms.

The analysis of Figure 4.2 provides several key insights into the behavior of effective thermal conductivity. The modified Zehner -Bauer (ZBS) correlation, enhanced with radiative heat transfer components, yielded an ETC increasing from 0.16 to 0.34 W/(m·.K) between 25-500°C. This near-exponential growth trend reflects the growing influence of thermal radiation at elevated temperatures. Among the models considered, the Zehner-Bauer model, which incorporates a contact area term between particles, shows only a minor increase in predicted ETC in contrast to the Zehner -Schlünder (ZS) model. This suggests that the particle contact area effect is insignificant on heat transfer for the specific sand grain size used in this study.

The Zehner-Damköhler correlation produces results similar to the other Zehner models, demonstrating consistency across different derivations. Meanwhile, the Yagi-Kunii and Kunii-Smith models tend to underestimate ETC at higher temperatures, as they do not fully capture the radiation contribution. The linear growth of k_s and k_f with temperature becomes more evident when radiation effects are included, introducing an exponential influence that becomes more pronounced under elevated temperature conditions, with increased particle diameters, or for materials exhibiting higher emissivity characteristics.

Due to the similarity among Zehner's radiative transfer models, Zehner-Bauer values are selected for further use in the COMSOL model, as they provide a more comprehensive representation of heat transfer in granular materials.

4.3 COMSOL Results for Heat Transfer Analysis

The COMSOL simulation inputs are comprehensively specified in Tables 3.1 through 3.3. Effective thermal conductivity values, completely imported from the Excel computational model, represent the only parameters varied across simulation iterations. The effect of implementing varying thermal conductivity models that include radiation effects: Zehner-Bauer, Kunii-Smith, and Yagi-Kunii within the COMSOL model at four different thermocouple locations is illustrated in Figure 4.3.

4.3.1 Heat transfer analysis at various locations of the sand-packed TES

Figure 4.3 suggests that the TES system undergoes a rapid heating phase before stabilizing, and the models effectively capture the thermal storage behavior with minimal deviation from the experimental data. Nearness to the heat source caused minimal variation in recorded temperatures among different correlation methods. The proximity of the measurement point to the heat source drives the Laplacian term ($\nabla^2 T$) to approach zero in the governing heat equation, thereby reducing the influence of TES thermal conductivity at this position. Initial model-measurement discrepancies at the heater location indicate potential oversimplification of the heating element representation in the COMSOL simulation framework.

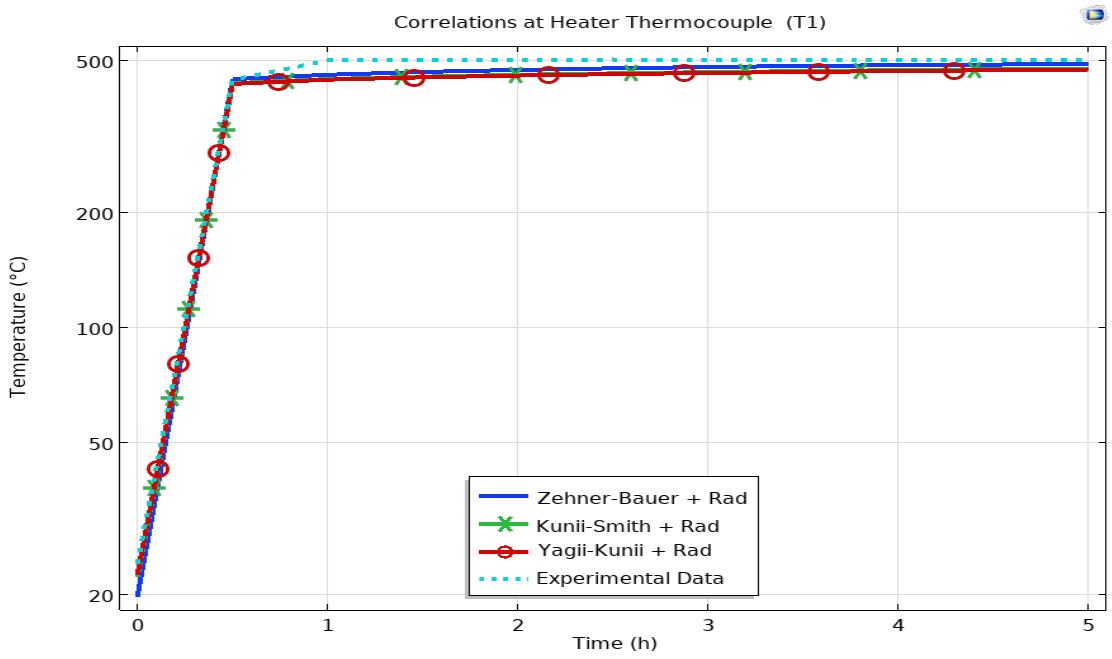

Figure 4.3: Impact of different correlations at heater thermocouple location (T1).

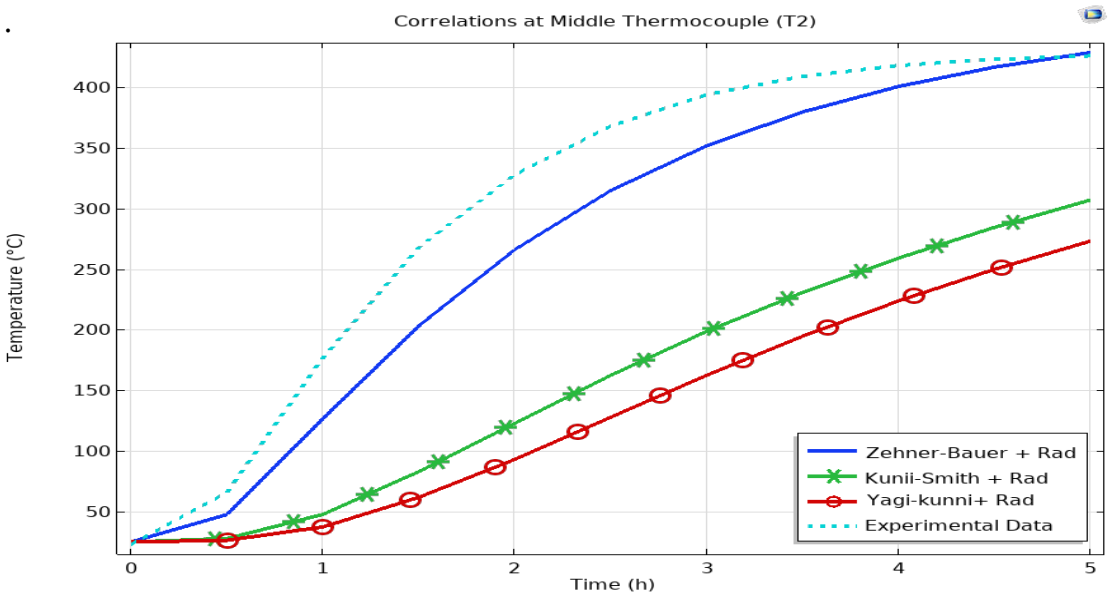

Figure 4.4: Impact of different correlations at the middle thermocouple location (T2) between two heaters.

Figure 4.4 clearly shows that correlations predicting higher thermal conductivity led to elevated temperatures at the middle thermocouple. This occurs because materials with higher conductivity result in more efficient heat transfer, causing the midpoint to reach the temperature of the heaters more rapidly. This trend is also evident for both outside points, as illustrated in Figure 4.5 and 4.6.

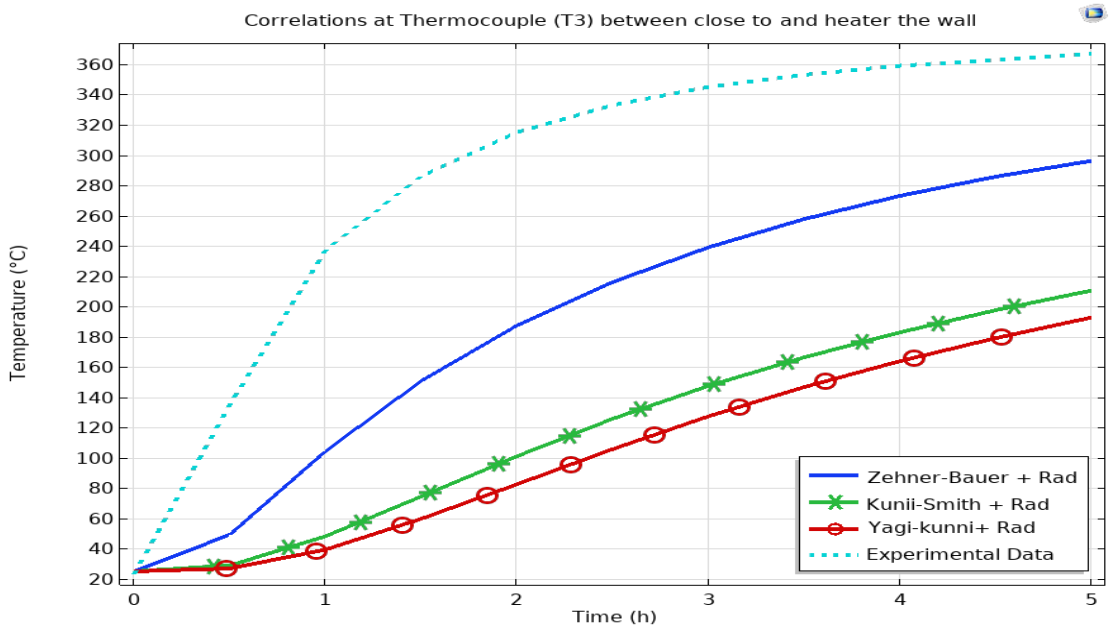

Figure 4.5: Impact of different correlations at the thermocouple location (T3) in between close to the heater and the boundary wall.

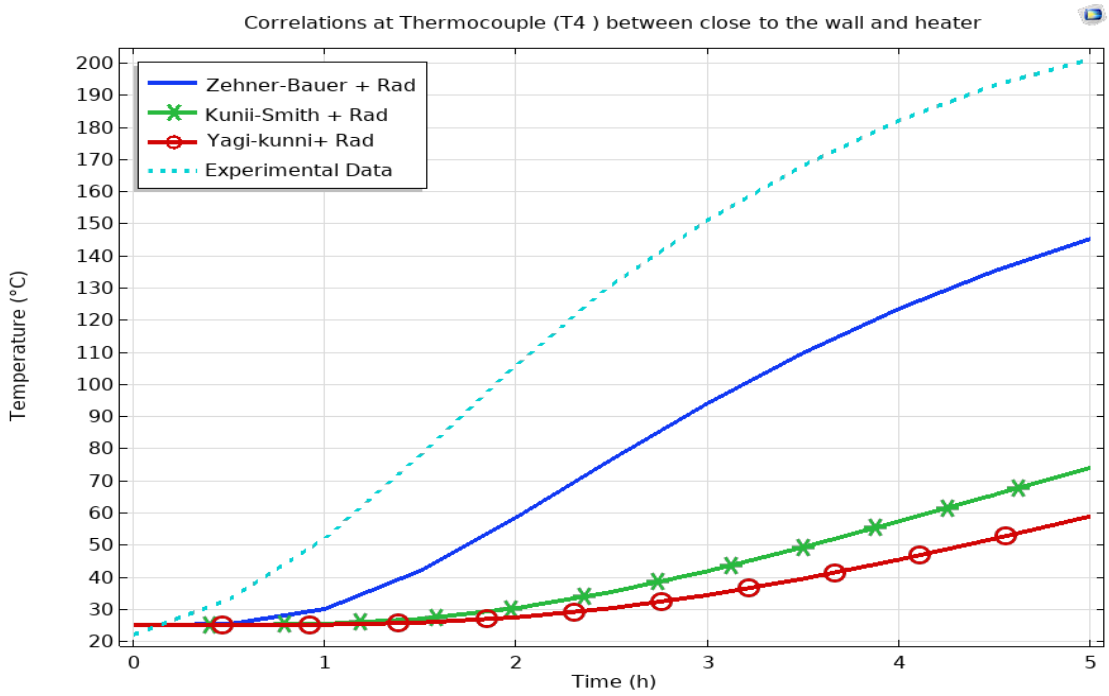

Figure 4.6: Impact of different correlations at the thermocouple location (T4) in between close to the boundary wall and the heater.

The third and fourth charts highlight significant deviations among the measured data and the three models and exhibited that Zehner-Bauer over-predicts, while Kunii-Smith and Yagi-Kunii under-predict heat storage performance. Among all evaluated correlations, the modified Zehner -Bauer formulation with radiative terms, considered to have higher thermal conductivity estimates, returned the closest agreement with experimental temperature measurements at every monitoring point. Interestingly, none of these effective thermal conductivity (ETC) correlations accurately predicted the measured data as indicated by the deviation seen in the figures. This suggests that the Yagi -Kunii and Kunii -Smith models may be more suitable for approximating the ETC at lower temperatures. These results are consistent with Botterill et al.'s research, suggesting that enhanced accuracy may be achievable through an ETC correlation exhibiting stronger temperature dependence, as evidenced by a steeper slope (Botterill et al., 1989).

4.3.2 Heatflux Distribution Pattern within sand packbed TES

The horizontally exploded view of the sand-packed TES system demonstrates effective heat distribution of the base case model Zehner -Bauer(ZB) correlation, with the radiative term, with high temperatures of 350^0C concentrated around the heating elements and gradual dissipation towards the periphery around 50^0C.

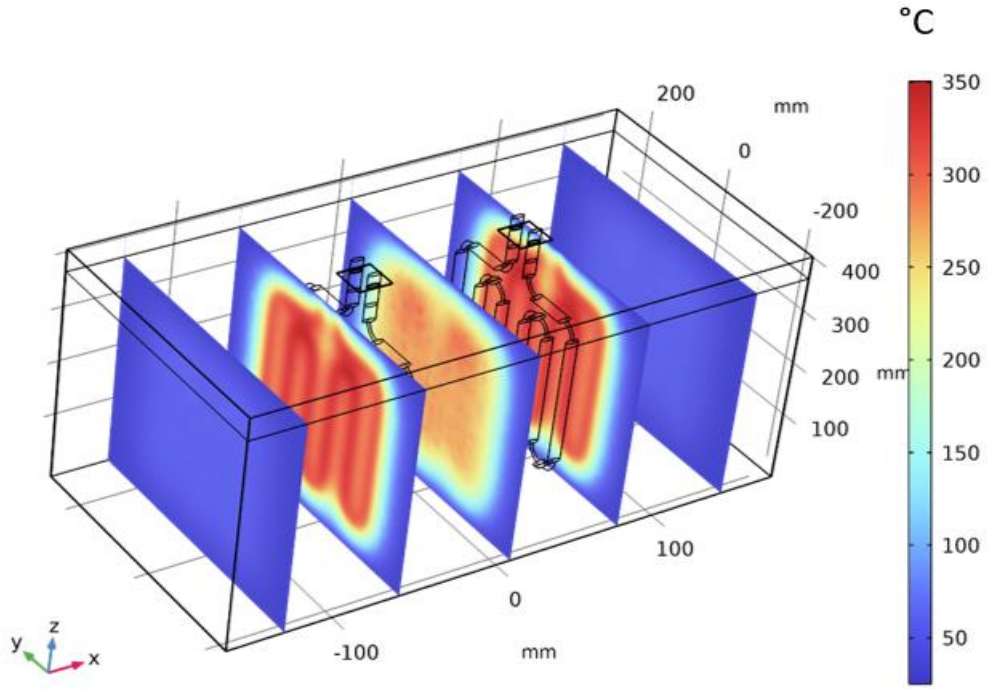

Figure 4.7: Horizontal exploded view of sand-packed bed TES during charging

The model effectively captures thermal conduction within the sand medium, though heat retention near the sources suggests potential optimization for more uniform distribution. Peripheral thermal losses indicate the need for improved insulation, while the layered structure facilitates heat transfer but may require adjustments to enhance efficiency. This further suggests design improvements by enhancing conduction pathways by embedding higher-conductivity materials to improve heat distribution and optimization of heating element placement to avoid localized overheating and enhance overall efficiency. The system appears well-suited for long-term storage of thermal energy, but improvements may be needed for faster heat retrieval. Further refinements in material selection, insulation, and heat exchanger design can enhance energy retention and retrieval, making it more effective for practical applications.

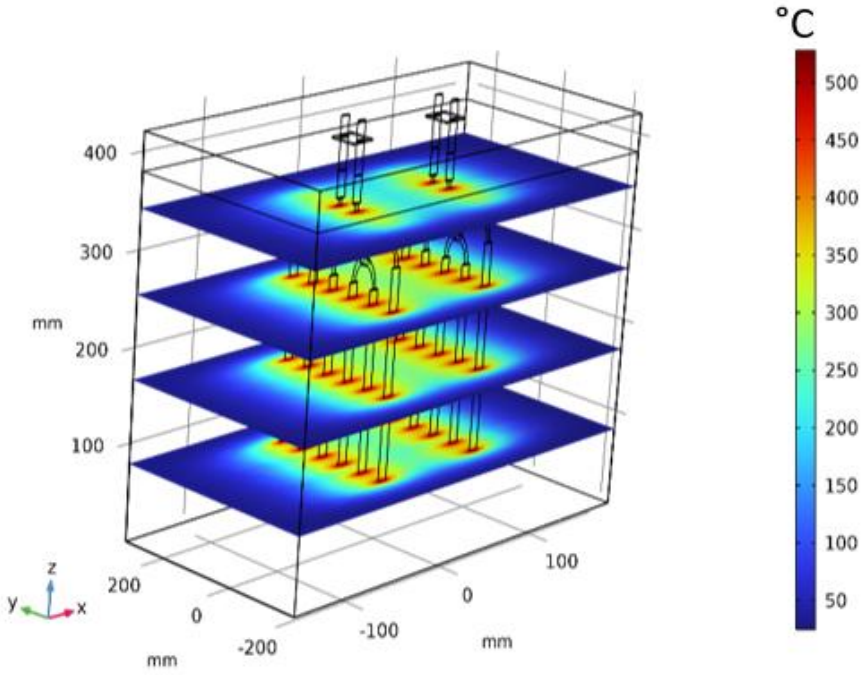

Figure 4.8: Vertical exploded view of sand-packed bed TES during charging

The vertically exploded view of the sand-packed TES system highlights efficient layered heat transfer in which temperature distribution is visualized using a color gradient, where red represents high temperatures of 500°C concentrated around the heating elements and blue represents lower temperatures 150°C representing gradual dissipation outwardly. The multi-layered structure represents vertical heat propagation through conduction and radiation, with lower layers heating up first before transferring energy to the upper layers. However, peripheral areas remain cooler, indicating potential thermal losses due to insufficient insulation. Additionally, improving the thermal conductivity of the packed material by incorporating higher-conductivity additives or optimizing particle size distribution can enhance heat transfer across layers and reduce thermal resistance.

4.4 Parametric Studies and Sensitivity Analysis

During charging, the temperature profile development of sand-filled TES systems depends on several variables, demanding a parametric investigation to evaluate critical contributing factors. This investigation was conducted using the COMSOL model, which focuses on identifying the effects of TES material property variations, including mass density, ETC, and heat capacity. The analysis further investigates thermal dissipation effects on temperature profiles through systematic variation of crucible surface emissivity (ε) and convective heat transfer coefficients (h) for TES-air boundary. Additionally, the analysis evaluates how thermal dissipation influences temperature distribution inside TES through systematic variations of crucible emissivity properties and TES boundary convection heat transfer coefficients.

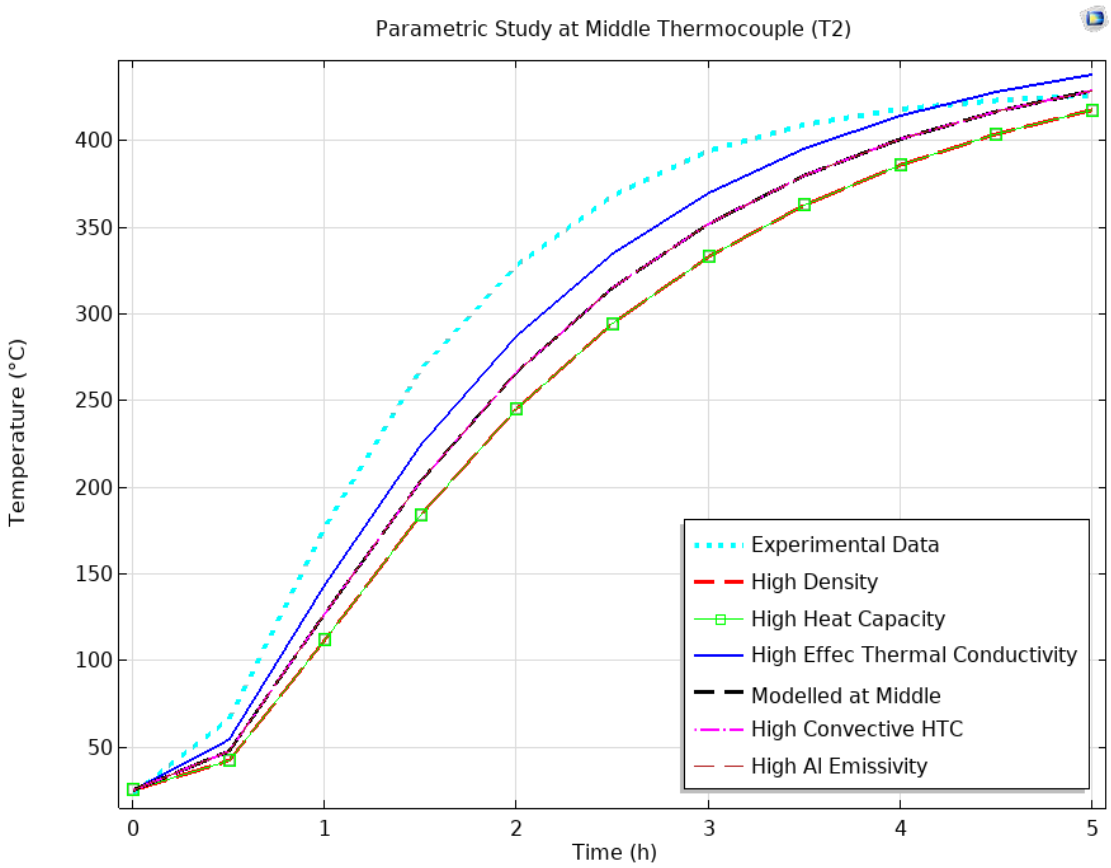

Figure 4.9: Comparison between the modeled temperature at the middle thermocouple location (T2) with the experimental data.

The base reference configuration employs parameters specified in Table 3.3, with ETC values calculated via the modified Zehner -Bauer radiation correlation in the Excel

framework. Comparative scenarios are created by increasing designated parameters by 10 percent above their tabulated baseline values.

Figure 4.9 shows that thermal conductivity is the most influential factor affecting temperature distribution. The ten percent increase in ETC of TES closely matched the experimental data throughout the curve in the modeled temperature at the middle region, indicating strong alignment where 10 percent enhancement in both density (ρ) and heat capacity (c_p) of the TES material leads to a significant temperature decrease at the central measurement location.

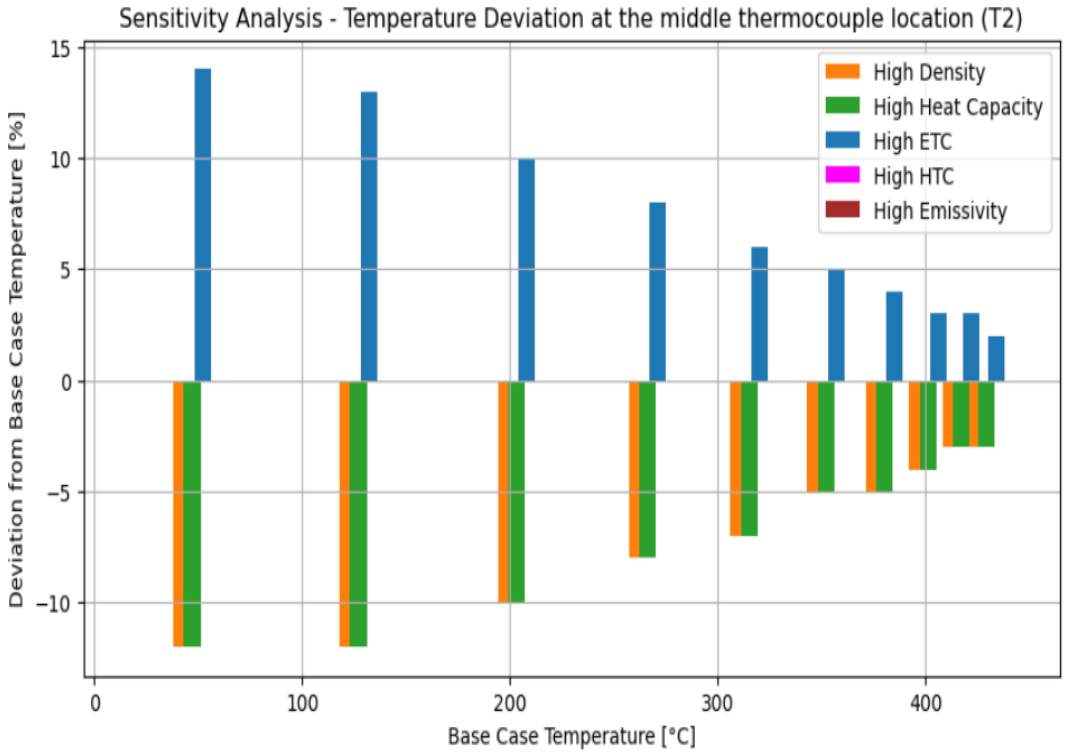

Figure 4.10: Sensitivity analysis of different parameters at the middle thermocouple location (T2).

Figure 4.10 demonstrates that the TES material's enhanced ETC exerts more influence during the initial charging phase, when a large amount of thermal energy is introduced during this time. As the system approaches thermal equilibrium with the heater and stabilizes, the energy input rate decreases, diminishing the parameter's relative impact. Therefore, increasing the ETC of the TES material improves charging rates while maintaining stable peak temperatures at the central region. Consequently, while enhanced ETC reduces charging time, its effect on the steady-state midpoint

temperature is negligible, as the system is thermally bounded by the heater's fixed 500°C limit.

Varying both the convective heat transfer parameter and radiative emissivity of the crucible by ten percent each has a minimal effect on the midpoint temperature compared to the previously discussed parameters. Notably, at elevated temperatures, higher crucible emissivity reduces the midpoint temperature due to increased radiative heat losses from the system. To mitigate this effect, additional insulation is recommended to minimize thermal losses. The investigation demonstrated that the ETC of TES materials directly impacts the energy transfer from the heater during charging. By carefully managing heat flux boundaries and minimizing thermal losses, the effects of intrinsic thermal conductivity can be analyzed more accurately.

4.5 Comparative Analysis of TES System Performance: Simulation versus Experimentation

A systematic evaluation of the thermal energy storage (TES) system was conducted through both numerical modeling and experimental validation, with key parameters and results summarized in Table 4.2. The study reveals important insights into system performance under simulated and actual operating conditions.

Table 4.2: Comparison of 3D model and experimental parameters

Parameter	3D Model	Experiment	Difference
Input energy (kWh)	10	9.9	-1.0%
Stored energy (kWh)	8.63	8.94	+3.6%
System efficiency (%)	86.26	90.33	+4.07%

The actual tests through the experimental setup showed 90.33 percent efficiency, which was 4.07 percent higher than the 3D simulation's 86.26 percent. The efficiency of the sand-packed bed TES system was evaluated through both 3D computational modeling and experimental testing.

In the 3D COMSOL model, a heater operating at 2000 W supplied energy for 5 hours, resulting in a total energy input of 10 kWh. The energy stored in the sand bed was calculated using the fundamental heat storage equation mentioned in equation 2.1, $Q_{stored} = m.C_p.\Delta T$, with temperature-dependent specific heat capacity and density mentioned in Table 3.3. The heat stored is the integral of $m.C_p(T)$ over the temperature and the mass was determined through volumetric estimation based on the system's geometry, resulting in an average stored energy of 8.63 kWh (31.05 MJ) and an efficiency of 86.26%.

The experimental setup, the heater drew 220 V and 9 A for the same duration, supplying 9.9 kWh of energy. The energy stored in the sand bed was calculated using the same heat storage equation with temperature-dependent specific heat capacity as mentioned earlier, and the heat stored is the integral of $m.C_p(T)$ over the temperature. Unlike the simulation, the sand mass was measured directly, eliminating volumetric

approximation errors. The experimental setup results in an average stored energy of 8.94 kWh (32.19 MJ), confirming superior real-world performance attributed to the elimination of volumetric estimation errors through direct mass measurement, improved thermal distribution characteristics in the actual system configuration, and a more precise representation of real-world operating conditions.

Both the simulation and experiments confirmed the sand-packed bed TES as a highly efficient (over 85 to 90 percent) sensible heat storage system, competitive with conventional solutions like molten salt (85 to 95 percent) and packed-rock beds (70 to 90 percent). However, the experimental results suggest that further refinements to the simulation, such as incorporating more precise power input parameters, could enhance model accuracy. This comparison not only validates the system's feasibility but also shows how real-world testing can help fine-tune simulations for better energy storage designs.

4.6 Thermal Conductivity Enhancement in Sand-Filled Thermal Storage

To enhance the sand-filled bed's thermal conductivity while maintaining minimal cost overhead, we started mixing aggregate from a layered mix to a uniform mix with sand and ended with mixing waste metal chips in a layer uniformly mixed with sand aggregate. Aggregate with sand and cast-iron metallic chips, with mixed sand aggregate, was examined. The experiments were conducted using aggregate used in building construction and sand, maintaining an aggregate-to-sand volume ratio of 1:3. Later the experiment was conducted using the same sand aggregate mix with cast iron metallic chips in layers, maintaining a metallic chips-to-sand-aggregate volume ratio of 1:11.8. Figures 4.11 represents the temperature variation over time at different locations in the Thermal Energy Storage (TES) system under different experimental configurations.

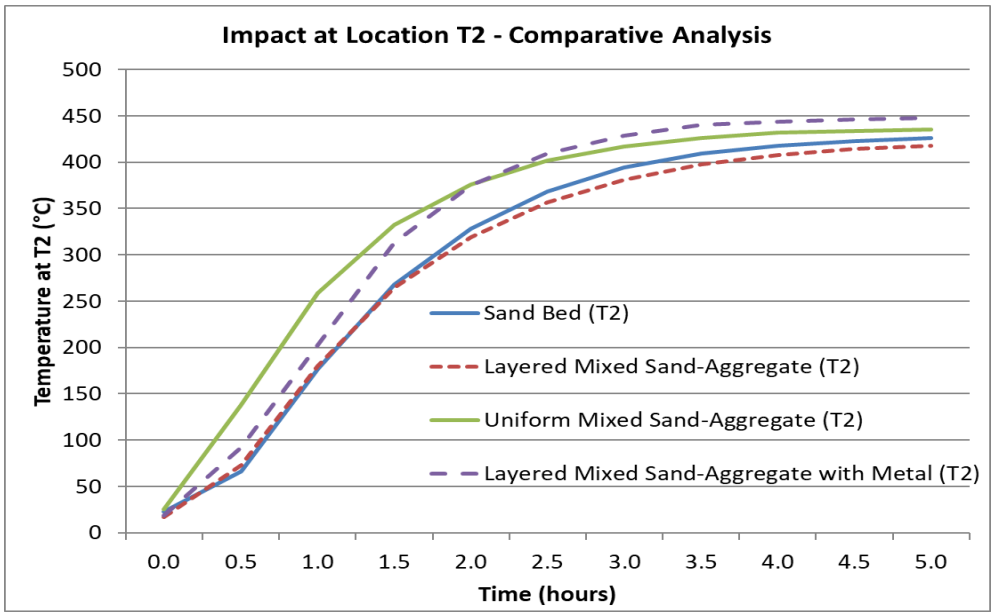

Figure 4.11: Different mixture variations at the middle thermocouple location (T2) between two heaters.

Here, the temperature at T2, which is the core region of TES, rises steadily across all configurations. Among them, the Layered Mixed Sand-Aggregate with Metal exhibits the fastest heat penetration, reaching the highest temperature, resulting from metallic materials' elevated thermal conductivity. The Uniform Mixed Sand-Aggregate heats up more quickly than both the Sand Bed and Layered Mixed Sand-Aggregate, but its final temperature stabilizes at a similar level. Meanwhile, the Layered Mixed Sand-

Aggregate initially heats up slower than the Sand Bed but eventually reaches a comparable temperature. Critically, the Layered Mixed Sand-Aggregate with Metal significantly enhances heat transfer, as expected from the presence of metal, while the Uniform Mixed Sand-Aggregate shows improved heat retention over time. However, the Layered Mixed Sand-Aggregate and Sand Bed perform almost identically, suggesting that layering alone does not provide a substantial advantage in heat transfer efficiency at this region.

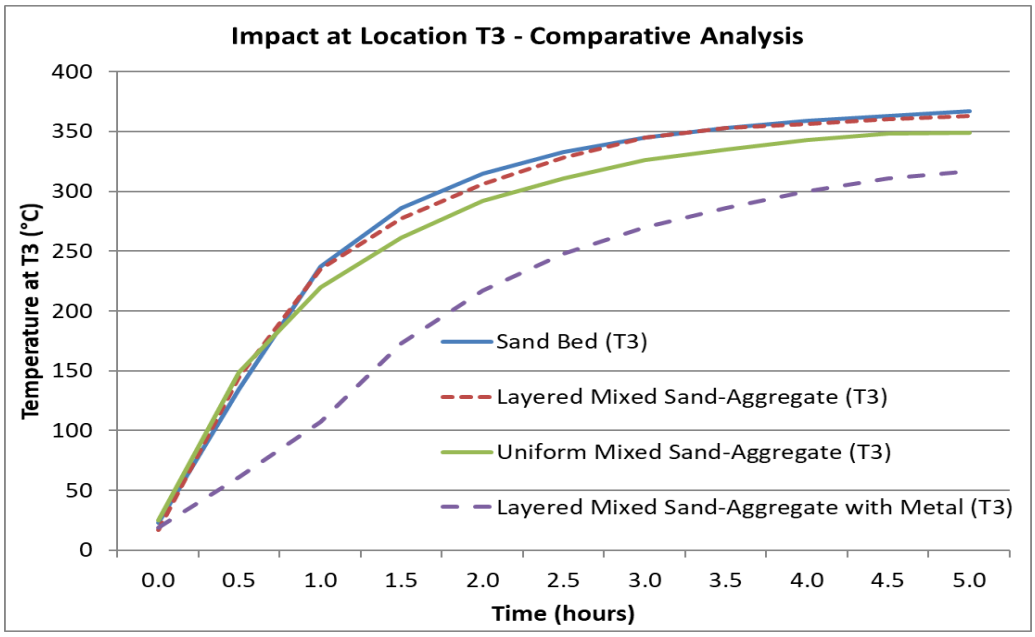

Figure 4.12: Different mixture variations at the thermocouple location (T3) in between close to the heater and the boundary wall.

In Figure 4.12, the temperature variations at the T3 region, which is between the wall and close to the heater, show that the sand bed and layered mixed sand aggregate exhibit nearly identical temperature profiles. The uniformly mixed sand aggregate initially heats up more slowly but eventually stabilizes at a slightly lower temperature. Notably, the layered mixed sand aggregate with metal chips records a significantly lower temperature at T3 compared to other configurations, suggesting that heat is being transferred more efficiently to other regions. Critically, this lower temperature in the layered mixed sand-aggregate with metal chips configuration is due to its higher thermal conductivity, allowing heat to disperse quickly. Meanwhile, the Sand Bed and layered mixed sand aggregate retain moderate amounts of heat, performing similarly.

The uniformly mixed sand-aggregate stabilizing at a slightly lower final temperature suggests potential inefficiencies in heat distribution within this setup.

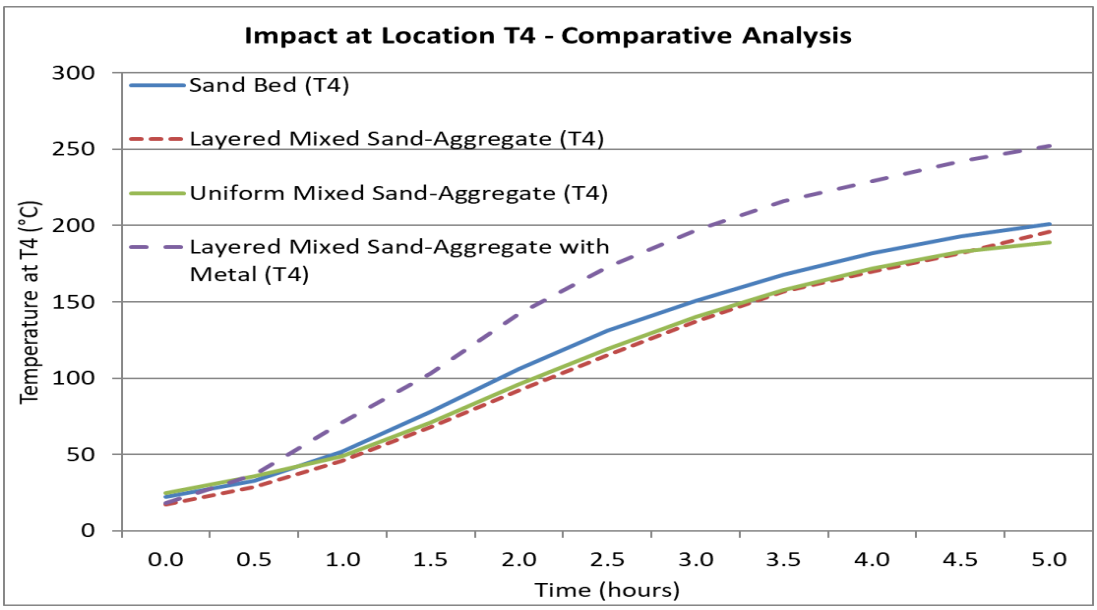

Figure 4.13: Different mixture variations at the thermocouple location (T4) in between close to the boundary wall and heater.

In Figure 4.13, the temperature variations at T4 region which is between the heater and close to the wall reveal that the sand bed and layered mixed sand-aggregate once again perform almost identically, maintaining similar temperature profiles. The uniformly mixed sand aggregate follows a comparable trend but remains slightly lower in temperature throughout. However, the layered mixed sand aggregate with Metal deviates significantly, displaying a much higher temperature profile than the other configurations. Critically, this elevated temperature in the layered mixed sand aggregate with metal is attributed to the high thermal conductivity of metal, which likely causes localized overheating in this region. The sand bed and layered mixed sand aggregate continue to perform consistently across different locations. Meanwhile, the uniform mixed sand aggregate shows slightly reduced efficiency at T4 compared to the core T2, suggesting variations in heat transfer behavior within this configuration.

This result showed that incorporating 7.8% cast iron metallic chips (by volume) layered into the sand-aggregate mixture improved heat transfer, increasing the center temperature of the TES from 416°C to 448°C compared to pure sand, demonstrating superior heat transfer, allowing for quicker heating. However, its high thermal conductivity also leads to significant heat dispersion, resulting in lower temperatures of

363°C at certain locations, such as T3. The uniformly mixed sand aggregate performs efficiently at the core but shows slightly reduced effectiveness near the walls, suggesting some limitations in heat retention. Metal composite cases achieve higher temperature levels compared to pure sand. While sand has a remarkably high temperature tolerance, its high thermal resistance makes efficient heat transfer difficult. However, the inclusion of metallic chips within the sand enhances heat conduction by creating efficient pathways for heat transfer, allowing for better utilization of the storage space. Meanwhile, the Sand Bed and layered mixed sand aggregate exhibit nearly identical performance, indicating that layering alone does not substantially impact heat distribution. For configuration selection, the layered mixed sand aggregate with metallic chips is ideal for rapid heating, while the uniformly mixed sand aggregate provides a more balanced heat distribution.

4.6.1 Thermal Performance of Layered Sand-Metal Composite TES

The TES with layered mixed sand aggregate with metallic chips was studied for 50 hours (0 to 49.5 hours) with temperature readings taken at different locations. The goal is to assess the TES system's heat retention capabilities and identify areas for future optimization based on the temperature data recorded across four different locations: Heater (T1), mid (T2), outside close to the heater (T3), and outside close to the wall (T4).

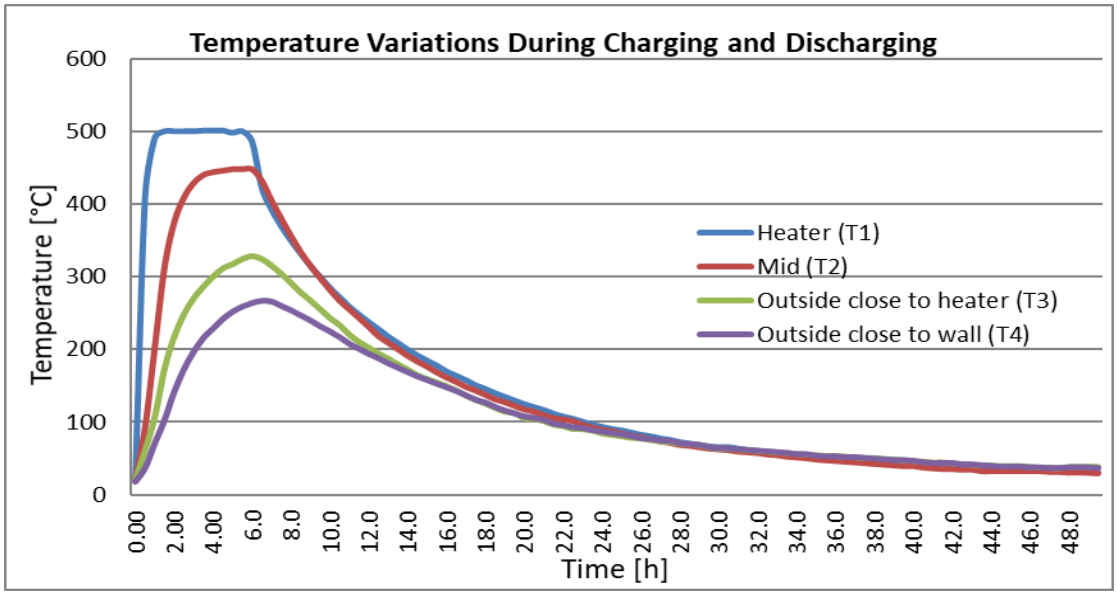

Figure 4.14: Temperature variations during charging and discharging of layered mixed sand aggregate with metallic chips.

During the charging phase (0–5 hours), the central thermocouple (T1) rapidly attained 500°C within 1.3 hours, corresponding to an initial heating rate of 369°C/h. The heater T1 heats the sand rapidly with a high charging rate of 96°C per hour. A thermal gradient across the system is observed, with temperatures decreasing as you move away from the heat source. The charging rate decreases, with T2 at 86°C per hour, T3 at 59.6°C per hour, and T4 at 46.8°C per hour as the distance from the heater increases. This temperature drop confirms the system maintains effective heat diffusion through the sand bed.

In the subsequent cooling phase (5–50 h), after the heater was turned off, the system exhibited a 1-hour thermal inertia period before temperature decline commenced. Notably, T4 temporarily increased by 12°C, suggesting internal heat redistribution. The central core (T2) retained the highest thermal energy, cooling from 448°C to 300°C, over 11 hours, while outer regions exhibited slower thermal dissipation. Specifically, T4 cooled at a rate of just 2.6°C/h after 12 hours, highlighting the system's effective heat retention and controlled release.

This behavior highlights the sand bed's intrinsic thermal retention properties, as temperatures decayed uniformly yet gradually. The delayed cooling in peripheral regions suggests that the system effectively minimizes thermal losses, making it suitable for long-duration energy storage. However, while the existing insulation contributes to heat preservation (evidenced by slower cooling at T3 and T4), further enhancements, such as integrating advanced insulation materials (e.g., aerogels, vacuum panels), could significantly reduce heat loss and extend thermal retention times.

CHAPTER FIVE: CONCLUSION AND RECOMMENDATION

5.1 Conclusion

A comprehensive numerical analysis was conducted to systematically examine heat transfer behavior in sand-filled TES using an advanced 3D simulation framework. It analyzed the governing equations to identify key parameters influencing the temperature variations in a sand-packed bed TES. Various modeling techniques were reviewed in the literature, among which the effective medium approximation proved most effective for simulating the system's granular thermal properties. To enhance understanding of heat transfer processes, different correlations for the effective thermal conductivity were systematically tested for agreement with empirical data, leading to these key findings:

a. This study demonstrates that the transient thermal distributions in the sand-filled based TES system are governed by the coupled effects of specific heat capacity, thermal conductivity, and density, alongside heat source effects, as quantified by Equation 2.2. Despite sand's advantageous thermal stability, its low intrinsic thermal conductivity significantly limits heat transfer efficiency. To overcome these limitations, we developed an experimental sand-bed TES apparatus coupled with computational modeling to investigate heat transfer mechanisms and identified performance enhancement strategies.
b. COMSOL Multiphysics simulations were employed to assess the thermal behavior of sand-filled TES thermal performance, confirming effective medium method is computationally efficient while accurately representing the granular medium. Among all the models tested, modified Zehner -Bauer (ZB) with radiative term showed the closest match to experimental results, especially at higher temperatures above 400°C. Parametric analyses confirmed that the thermal conductivity of TES materials plays a crucial role in determining the efficiency of energy transfer from the heater to the bed, which ranged between 85% and 90% during charging. Both numerical simulations and experimental findings validated the sand-filled bed as a highly efficient sensible heat storage system, comparable to traditional TES solutions.

c. The study developed low-cost thermal conductivity enhancement in sand-based TES by incorporating waste cast iron metallic chips. Among the tested configurations, a layered arrangement of 7.8% cast iron chips (by volume) within the sand-aggregate bed yielded optimal performance, increasing the core temperature by 32°C (from 416°C to 448°C) during charging while retaining more than 85% thermal efficiency. The metallic chips formed conductive networks, improving heat transfer without sacrificing the sand's inherent thermal retention capacity, verified through post-heating decay analysis. These findings demonstrate that strategically layered low-cost additives can economically optimize TES performance by balancing enhanced conductivity with sustained energy release.

5.2 Recommendation

Based on the research, the following are the major recommendations:

- Future research should explore alternative high-conductivity materials beyond metallic chips, such as ceramic-metal composites, which may offer improved thermal performance and durability. It is also essential to investigate the long-term stability and thermal cycling effects of different composite mixtures to ensure sustained performance over multiple charge-discharge cycles.
- Advancing modeling and validation techniques will further improve the accuracy of TES simulations. The COMSOL model should be expanded to incorporate fully electrothermal energy storage (ETES) systems, integrating both thermal and electrical storage components. Moreover, refining the Zehner -Bauer correlation at high temperatures leads to better predictive accuracy.
- Lastly, to ensure the practicality of these theoretical improvements, large-scale experimental validation is necessary. A full-scale TES prototype with a heat retrieval mechanism should be developed to test system performance under real operating conditions. Understanding heat loss mechanisms and optimizing insulation techniques will be crucial for improving energy retention. Furthermore, experimental studies should examine various charging and discharging cycles to evaluate the long-term stability and efficiency of the TES system, ensuring it can meet practical energy storage demands.

REFERENCES

Al-Ghussain, L., Darwish Ahmad, A., Abubaker, A. M., & Hassan, M. A. (2022). Techno-economic feasibility of thermal storage systems for the transition to 100% renewable grids. *Renewable Energy*, *189*, 800–812. https://doi.org/https://doi.org/10.1016/j.renene.2022.03.054

Alva, G., Lin, Y., & Fang, G. (2018). An overview of thermal energy storage systems. *Energy*, *144*, 341–378. https://doi.org/https://doi.org/10.1016/j.energy.2017.12.037

Alva, G., Liu, L., Huang, X., & Fang, G. (2017). Thermal energy storage materials and systems for solar energy applications. *Renewable and Sustainable Energy Reviews*, *68*, 693–706. https://doi.org/https://doi.org/10.1016/j.rser.2016.10.021

Botterill, J. S. M., Salway, A. G., & Teoman, Y. (1989). The effective thermal conductivity of high temperature particulate beds—II. Model predictions and the implication of the experimental values. *International Journal of Heat and Mass Transfer*, *32*(3), 595–609. https://doi.org/https://doi.org/10.1016/0017-9310(89)90147-6

Calvin, K., Dasgupta, D., Krinner, G., Mukherji, A., Thorne, P. W., Trisos, C., Romero, J., Aldunce, P., Barrett, K., Blanco, G., Cheung, W. W. L., Connors, S., Denton, F., Diongue-Niang, A., Dodman, D., Garschagen, M., Geden, O., Hayward, B., Jones, C., … Ha, M. (2023). *IPCC, 2023: Climate Change 2023: Synthesis Report. Contribution of Working Groups I, II and III to the Sixth Assessment Report of the Intergovernmental Panel on Climate Change [Core Writing Team, H. Lee and J. Romero (eds.)]. IPCC, Geneva, Switzerland.* (P. Arias, M. Bustamante, I. Elgizouli, G. Flato, M. Howden, C. Méndez-Vallejo, J. J. Pereira, R. Pichs-Madruga, S. K. Rose, Y. Saheb, R. Sánchez Rodríguez, D. Ürge-Vorsatz, C. Xiao, N. Yassaa, J. Romero, J. Kim, E. F. Haites, Y. Jung, R. Stavins, … C. Péan, Eds.). https://doi.org/10.59327/IPCC/AR6-9789291691647

Chen, T., Jin, Y., Lv, H., Yang, A., Liu, M., Chen, B., Xie, Y., & Chen, Q. (2020). Applications of Lithium-Ion Batteries in Grid-Scale Energy Storage Systems.

Transactions of Tianjin University, *26*(3), 208–217. https://doi.org/10.1007/s12209-020-00236-w

Diago, M., Iniesta, A. C., Delclos, T., Soum-Glaude, A., Shamim, T., & Calvet, N. (2016). Characterization of desert sand as a sensible thermal energy storage medium. *AIP Conference Proceedings*, *1734*(1), 050011. https://doi.org/10.1063/1.4949109

Díaz-Heras, M., Belmonte, J. F., & Almendros-Ibáñez, J. A. (2020). Effective thermal conductivities in packed beds: Review of correlations and its influence on system performance. *Applied Thermal Engineering*, *171*, 115048. https://doi.org/https://doi.org/10.1016/j.applthermaleng.2020.115048

Dinçer, I., & Rosen, M. A. (2010). Thermal Energy Storage: Systems and Applications, Second Edition. *Thermal Energy Storage: Systems and Applications, Second Edition*. https://doi.org/10.1002/9780470970751

emissivities. (n.d.). Retrieved February 12, 2025, from https://www.vulcanelectric.com/wp-content/uploads/2017/08/emissivities.pdf

Greenspec. (2024). *GreenSpec: Energy Efficiency: Thermal Storage for Water Heating*. https://www.greenspec.co.uk/building-design/thermal-storage/

Hamdhan, I. N., & Clarke, B. G. (2010). Determination of Thermal Conductivity of Coarse and Fine Sand Soils. In *Proceedings World Geothermal Congress*.

Howlader, M., Rashid, M., Mallick, D., & Haque, T. (2012). Effects of aggregate types on thermal properties of concrete. *ARPN Journal of Engineering and Applied Sciences*, *7*, 900–907.

Hsu, C. T., Cheng, P., & Wong, K. W. (1994). Modified Zehner-Schlunder models for stagnant thermal conductivity of porous media. *International Journal of Heat and Mass Transfer*, *37*(17), 2751–2759. https://doi.org/https://doi.org/10.1016/0017-9310(94)90392-1

IEA. (2023). *World Energy Outlook 2023*. www.iea.org/terms

IRENA. (2023). *World energy transitions outlook 2023 : 1.5°C pathway*. International Renewable Energy Agency IRENA.

Ižvolt, L., & Dobeš, P. (2014). Test Procedure Impact for the Values of Specific Heat Capacity and Thermal Conductivity Coefficient. *Procedia Engineering*, *91*. https://doi.org/10.1016/j.proeng.2014.12.025

Kadoya, K., Matsunaga, N., & Nagashima, A. (1985). Viscosity and Thermal Conductivity of Dry Air in the Gaseous Phase. *Journal of Physical and Chemical Reference Data*, *14*(4), 947–970. https://doi.org/10.1063/1.555744

Kebede, A. A., Kalogiannis, T., Van Mierlo, J., & Berecibar, M. (2022). A comprehensive review of stationary energy storage devices for large scale renewable energy sources grid integration. *Renewable and Sustainable Energy Reviews*, *159*, 112213. https://doi.org/https://doi.org/10.1016/j.rser.2022.112213

Kunii, D., & Smith, J. M. (1960). Heat transfer characteristics of porous rocks. *AIChE Journal*, *6*(1), 71–78. https://doi.org/https://doi.org/10.1002/aic.690060115

Laubscher, H. F., Von Backström, T. W., & Dinter, F. (2017). Developing a cost effective rock bed thermal energy storage system: Design and modelling. *AIP Conference Proceedings*, *1850*. https://doi.org/10.1063/1.4984436

Liang, T., Vecchi, A., Knobloch, K., Sciacovelli, A., Engelbrecht, K., Li, Y., & Ding, Y. (2022). Key components for Carnot Battery: Technology review, technical barriers and selection criteria. *Renewable and Sustainable Energy Reviews*, *163*, 112478. https://doi.org/https://doi.org/10.1016/j.rser.2022.112478

Lin, L., Wang, L., Bai, Y., Lin, X., Zhang, S., Ge, Z., Peng, L., & Chen, H. (2023). Experimental study on the storage performance of the innovative spray-type packed bed thermal energy storage. *Applied Thermal Engineering*, *219*, 119415. https://doi.org/https://doi.org/10.1016/j.applthermaleng.2022.119415

Lou, W., Luo, L., Hua, Y., Fan, Y., & Du, Z. (2021). A review on the performance indicators and influencing factors for the thermocline thermal energy storage systems. In *Energies* (Vol. 14, Issue 24). MDPI. https://doi.org/10.3390/en14248384

Magnesium Oxide MgO Optical Material | Crystran. (n.d.). Retrieved February 12, 2025, from https://www.crystran.com/optical-materials/magnesium-oxide-mgo

Mahfoudi, N., Moummi, A., & Ganaoui, M. El. (2014). Sand as a heat storage media for a solar application: Simulation results. *Applied Mechanics and Materials*, *621*, 214–220. https://doi.org/10.4028/www.scientific.net/AMM.621.214

material-properties.org. (n.d.). Retrieved February 13, 2025, from https://material-properties.org/sand-density-heat-capacity-thermal-conductivity/

Mitali, J., Dhinakaran, S., & Mohamad, A. A. (2022). Energy storage systems: a review. In *Energy Storage and Saving* (Vol. 1, Issue 3, pp. 166–216). Elsevier B.V. https://doi.org/10.1016/j.enss.2022.07.002

Olivetti, E. A., Ceder, G., Gaustad, G. G., & Fu, X. (2017). Lithium-Ion Battery Supply Chain Considerations: Analysis of Potential Bottlenecks in Critical Metals. In *Joule* (Vol. 1, Issue 2, pp. 229–243). Cell Press. https://doi.org/10.1016/j.joule.2017.08.019

Polar Night Energy. (n.d.-a). *Sand Battery - Polar Night Energy*. Retrieved December 19, 2024, from https://polarnightenergy.com/sand-battery/

Polar Night Energy. (n.d.-b). *What is a sand battery? — Polar Night Energy*. Retrieved August 3, 2024, from https://polarnightenergy.fi/sand-battery

Qian, Y., Han, Z., Zhan, J.-H., Liu, X., & Xu, G. (2018). Comparative evaluation of heat conduction and radiation models for CFD simulation of heat transfer in packed beds. *International Journal of Heat and Mass Transfer*, *127*, 573–584. https://doi.org/https://doi.org/10.1016/j.ijheatmasstransfer.2018.06.127

Quartz. (n.d.). Retrieved January 29, 2025, from http://hyperphysics.phy-astr.gsu.edu/hbase/Geophys/quartz.html

Shi, Y., Chen, X., Sun, C., & Xia, X.-L. (2023). Temperature-Dependent Thermal Conductivity and Absorption Coefficient Identification of Quartz Window up to 1100 K. *Journal of Thermal Science*, *32*(1), 44–58. https://doi.org/10.1007/s11630-022-1747-x

Sih, S. S., & Barlow, J. W. (n.d.). *THE PREDICTION OF TlIE TIlERMAL CONDUCTIVITY OF POWDERS*.

Specific Heat of common Substances. (n.d.). Retrieved February 12, 2025, from https://www.engineeringtoolbox.com/specific-heat-capacity-d_391.html

Stephan, K., & Laesecke, A. (1985). The Thermal Conductivity of Fluid Air. *Journal of Physical and Chemical Reference Data*, *14*(1), 227–234. https://doi.org/10.1063/1.555749

Sunku Prasad, J., Muthukumar, P., Desai, F., Basu, D. N., & Rahman, M. M. (2019). A critical review of high-temperature reversible thermochemical energy storage systems. *Applied Energy*, *254*, 113733. https://doi.org/https://doi.org/10.1016/j.apenergy.2019.113733

Surface Emissivity Coefficients. (n.d.). Retrieved February 12, 2025, from https://www.engineeringtoolbox.com/emissivity-coefficients-d_447.html

Tavman, I. H. (1996). Effective thermal conductivity of granular porous materials. *International Communications in Heat and Mass Transfer*, *23*(2), 169–176. https://doi.org/https://doi.org/10.1016/0735-1933(96)00003-6

Tetteh, S., Yazdani, M. R., & Santasalo-Aarnio, A. (2021). Cost-effective Electro-Thermal Energy Storage to balance small scale renewable energy systems. *Journal of Energy Storage*, *41*, 102829. https://doi.org/https://doi.org/10.1016/j.est.2021.102829

Tsotsas, E., & Martin, H. (1987). Thermal conductivity of packed beds: A review. *Chemical Engineering and Processing: Process Intensification*, *22*(1), 19–37. https://doi.org/https://doi.org/10.1016/0255-2701(87)80025-9

Villasmil, W., Fischer, L. J., & Worlitschek, J. (2019). A review and evaluation of thermal insulation materials and methods for thermal energy storage systems. *Renewable and Sustainable Energy Reviews*, *103*, 71–84. https://doi.org/https://doi.org/10.1016/j.rser.2018.12.040

Yagi, S., & Kunii, D. (1957). Studies on effective thermal conductivities in packed beds. *Aiche Journal*, *3*, 543–546. https://api.semanticscholar.org/CorpusID:102085443

Zavattoni, S., Barbato, M., Zavattoni, S. A., Barbato, M. C., Pedretti, A., Zanganeh, G., & Steinfeld, A. (2012). *Effective thermal conductivity and axial porosity distribution of a rock-bed TES system: CFD modeling and experimental validation*. https://www.researchgate.net/publication/250951688

APPENDIX

1. The efficiency of 3D computational modeling of the sand-packed bed TES system

To calculate input energy (Wh), Q = P X T,

Heater Capacity = 2000 W

Heat supplied duration = 5 h

Input energy = 10 kWh

To calculate stored energy (Wh),

As per Geometric Design, Volume (V) = 0.0773 m^3

As per Table 4.1, Density (ρ) = 1425 kg/m^3

Mass (m) = ρ × V = 110.2 kg

Defining Cp(T) as a linear function, ranging from 776 J/kg·K at 60°C to 1133 J/kg·K at 500°C as of Table 3.3.

$$Cp(T) = 776 + \left(\frac{1133 - 776}{500 - 60}\right)(T - 60) = 776 + 0.8114\ (T - 60)$$

Calculating the heat stored at each thermocouple with an initial temperature of 25°C,

$$Q_i = m \int_{T_0}^{T_i(t)} Cp(T)\ dT$$

$$Q_i = m\ \left[776\ (T_i - T_0) + \frac{0.8114}{2}\ ((T_i - 60)^2 - (T_0 - 60)^2)\right]$$

$$Q_i = 110.2\ [776(T_i - 25) + 0.4057\ ((T_i - 60)^2 - 1225)]$$

Calculating the heat stored at each thermocouple location to find out the efficiency

Thermocouple Location	Final Temperature	Heat Stored, Q_i in (MJ)	Average Heat Stored (MJ)	Heat Stored (KWh)	Efficiency of the 3D Model (%)
T_1 (Heater)	487	47.60	31.05	8.63	86.26%
T_2 (Core)	428	40.46			
T_3 (Mid)	296	25.61			
T_4 (Wall)	145	10.53			

2. The efficiency of the experiment setup of the sand-packed bed TES system

To calculate Input energy (Wh), Q= P X T = V X I X T, (the heater draws 220V, 9-amp current for 5 hours)

Voltage, V = 220 V

Current, I = 9 A

Time, T = 5 h

Input energy = 9.9 kWh

To calculate stored energy (Wh),

Measured Mass (m) = 101.8 kg

Defining Cp(T) as a linear function, ranging from 776 J/kg·K at 60°C to 1133 J/kg·K at 500°C as of Table 3.3.

$$Cp(T) = 776 + \left(\frac{1133 - 776}{500 - 60}\right)(T - 60) = 776 + 0.8114\,(T - 60)$$

Calculating the heat stored at each thermocouple with an initial temperature of 23°C,

$$Q_i = m \int_{T_0}^{T_i(t)} Cp(T)\, dT$$

$$Q_i = m \left[776\,(T_i - T_0) + \frac{0.8114}{2}\,((T_i - 60)^2 - (T_0 - 60)^2)\right]$$

$$Q_i = 101.8\,[776(T_i - 23) + 0.4057\,((T_i - 60)^2 - 1369)]$$

Calculating the heat stored at each thermocouple location to find out the efficiency

Thermocouple Location	Final Temperature	Heat Stored, Q_i in (MJ)	Average Heat Stored (MJ)	Heat Stored (KWh)	Efficiency of the Experiment Setup (%)
T_1 (Heater)	500	45.62	32.19	8.94	90.33
T_2 (Core)	426	37.31			
T_3 (Mid)	367	31.01			
T_4 (Wall)	201	14.83			

Surendra Gurung

Modeling & Analyzing Heat Transfer Behavior of Sand-Packed Bed Thermal Energy Storage System

Tribhuvan University

Document Details

Submission ID
trn:oid:::3117:449433311

Submission Date
Apr 15, 2025, 10:41 PM GMT+5:45

Download Date
Apr 15, 2025, 10:44 PM GMT+5:45

File Name
Final Thesis Report after format - Surendra Gurung.docx

File Size
7.6 MB

56 Pages

11,530 Words

70,111 Characters

iThenticate Page 1 of 60 - Cover Page Submission ID trn:oid:::3117:449433311

2% Overall Similarity

The combined total of all matches, including overlapping sources, for each database.

Filtered from the Report

- Bibliography
- Quoted Text
- Cited Text
- Small Matches (less than 8 words)

Match Groups

- **28** Not Cited or Quoted 2%
  Matches with neither in-text citation nor quotation marks
- **0** Missing Quotations 0%
  Matches that are still very similar to source material
- **0** Missing Citation 0%
  Matches that have quotation marks, but no in-text citation
- **0** Cited and Quoted 0%
  Matches with in-text citation present, but no quotation marks

Top Sources

2% Internet sources
1% Publications
0% Submitted works (Student Papers)

Integrity Flags

1 Integrity Flag for Review

Hidden Text
53 suspect characters on 17 pages
Text is altered to blend into the white background of the document.

Our system's algorithms look deeply at a document for any inconsistencies that would set it apart from a normal submission. If we notice something strange, we flag it for you to review.

A Flag is not necessarily an indicator of a problem. However, we'd recommend you focus your attention there for further review.

Match Groups

- 28 Not Cited or Quoted 2%
  Matches with neither in-text citation nor quotation marks
- 0 Missing Quotations 0%
  Matches that are still very similar to source material
- 0 Missing Citation 0%
  Matches that have quotation marks, but no in-text citation
- 0 Cited and Quoted 0%
  Matches with in-text citation present, but no quotation marks

Top Sources

2% Internet sources
1% Publications
0% Submitted works (Student Papers)

Top Sources

The sources with the highest number of matches within the submission. Overlapping sources will not be displayed.

1	Publication	Sampson Tetteh, Gabriel Juul, Mika Järvinen, Annukka Santasalo-Aarnio. "Improv... <1%
2	Internet	scholar.sun.ac.za <1%
3	Internet	aaltodoc.aalto.fi <1%
4	Internet	dlib.hust.edu.vn:8080 <1%
5	Internet	docslib.org <1%
6	Internet	products.ihserc.com <1%
7	Publication	Taha Zakaraia Abdel Wahid, Zaki Mrzog Alaofi, Taha Radwan. "On mathematical a... <1%
8	Internet	erepository.uoeld.ac.ke <1%
9	Internet	export.arxiv.org <1%
10	Internet	www.gcw.nl <1%

11	Internet	
www.tutorialspoint.com		<1%
12	Internet	
etd.aau.edu.et		<1%
13	Internet	
mts.intechopen.com		<1%
14	Internet	
riunet.upv.es		<1%
15	Internet	
uwspace.uwaterloo.ca		<1%
16	Internet	
www.hindawi.com		<1%
17	Publication	
"Proceedings of the RILEM Spring Convention and Conference 2024", Springer Sci...		<1%
18	Publication	
Faisal Al-Juwayhel, Hisham El-Dessouky, Hisham Ettouney. "Analysis of single-effe...		<1%
19	Publication	
Fang, Yuan. "Experimental and Numerical Analysis of Light-Emitting Diode (LED) ...		<1%
20	Publication	
H.T. Aichlmayr, F.A. Kulacki. "The Effective Thermal Conductivity of Saturated Por...		<1%
21	Internet	
backend.orbit.dtu.dk		<1%
22	Internet	
scholarworks.iupui.edu		<1%
23	Internet	
theses.hal.science		<1%

Gmail

Surendra Gurung <sungrg777@gmail.com>

[IOEGC16] Editor Decision

1 message

Kobid <conference-noreply@ioe.edu.np> Sat, Mar 29, 2025 at 5:17 PM
To: surendra gurung <sungrg777@gmail.com>

surendra gurung:

We are pleased to inform you that your manuscript titled "Modeling And Analyzing Heat Transfer Behavior of Sand Packed Bed Thermal Energy Storage System" submitted to 16th IOE Graduate Conference is **Accepted** for presentation in the Conference as well as inclusion in the Peer-Reviewed Proceedings. Please note that inclusion in hard copy proceedings is contingent upon your timely response to further edits, if any, during the publication process.

Reviewer's Comments:

Thank you authors for revision of the manuscripts as per the comments.

With Warm Regards,
IOEGC-16 Editorial Team